JOURNAL OF GEOPHYSICAL RESEARCH, VOL. 105, NO. D7, PAGES 8981–9002, APRIL 16, 2000

The modeling of tropospheric methane: How well can point measurements be reproduced by a global model?

Sander Houweling, Frank Dentener, and Jos Lelieveld
Institute for Marine and Atmospheric Research Utrecht, Utrecht University, Utrecht, Netherlands

Bernadette Walter
Columbia University/NASA Goddard Institute for Space Studies, New York

Ed Dlugokencky
NOAA Climate Monitoring and Diagnostics Laboratory, Boulder, Colorado

Abstract. Global model simulations of tropospheric methane are presented, using state of the art representations of its terrestrial sources. Parameters critical for its tropospheric sink and transport have been evaluated using CH_3CCl_3 and SF_6. We assess how well available methane measurements can be reproduced by the model, and how model and measurements can most efficiently be compared. Using European Centre for Medium-Range Weather Forecasts reanalyzed meteorological fields, direct comparisons between model results and flask or in situ measurements are presented, as opposed to comparing multiannual averaged seasonal cycles and trends as was done in previous studies. When comparing monthly means derived from weekly flask sampling and the model, the agreement at stations as Bermuda East and Mace Head is improved if, instead of sampling the model at each model time step, samples are taken at the same times as the measurements were taken. A method is presented to estimate the potential influence of subgrid variability using a marked tracer that is emitted in the vicinity of observational stations only. From the contribution of this tracer to the computed methane concentration at a particular station, the potential contribution of subgrid sources can be estimated. Radon 222 is used to select baseline conditions in the model to improve the comparability of model and measurements when a clean air sector is selected for sampling. Comparisons of model results and measurements, screened for local influences and artifacts of wind sector selection, indicate that the model has in particular difficulty reproducing seasonal cycles at higher latitude stations of the Northern Hemisphere. Sensitivity simulations show that the simulated annual variation at these stations is sensitive to the parameterization of wetland emissions. Also at the South China Sea, model simulations point to errors in the representation of methane sources. Marked tracer simulations indicate that this is most likely related to emissions from natural wetlands and rice paddies, in line with recent inverse modeling and up-scaling estimates.

1. Introduction

Methane is an important trace gas in the Earth's atmosphere. It is the second most important increasing greenhouse gas, with an estimated contribution to the present climate forcing of 35% of that by increasing CO_2 [*Lelieveld et al.*, 1998]. This is associated with absorption of longwave radiation (mainly at λ=7.6 μm), and indirect warming by tropospheric ozone and stratospheric water vapor, that are products of its oxidation. Further, methane influences the lifetimes of various chemically reactive trace gases owing to a photochemical feedback on the hydroxyl radical [*Crutzen and Zimmerman*, 1991; *Krol et al.*, 1998].

Tropospheric methane concentrations are monitored by several measurement networks starting about two decades ago [*Dlugokencky et al.*, 1994b; *World Meteorological Organization*, 1997; *GLOBALVIEW-CH_4*, 1999]. Since methane is relatively evenly distributed over the globe, owing to a tropospheric residence time of about 8 years [*Lelieveld et al.*, 1998], these measurements quite well constrain its tropospheric abundance. On the other hand, sources and sinks of methane are relatively weakly constrained. As a consequence, it is difficult to understand the time evolution of methane [*Dlugokencky et al.*, 1994a, 1996, 1998] and anticipate future changes.

To improve our understanding of the present methane budget, modelers have tried to integrate all available informa-

Copyright 2000 by the American Geophysical Union.

Paper number 1999JD901149.
0148-0227/00/1999JD901149$09.00

tion on sources, sinks and observed concentrations, using either forward [*Fung et al.*, 1991; *Lelieveld et al.*, 1998] or inverse techniques [*Brown*, 1993; *Hein et al.*, 1997; *Kandlikar*, 1997; *Saeki et al.*, 1998; *Houweling et al.*, 1999]. Inverse modeling is a useful tool to relate accurate methane concentration measurements to relatively uncertain sources and sinks. Previous inversions of methane and of other long-lived trace gases such as CO_2 indicate, however, that a large number of measurements are required to substantially constrain fluxes since their smooth concentration distributions render the inverse problem ill-conditioned. In addition, model errors may seriously affect emission estimates derived by inverse modeling [*Houweling et al.*, 1999]. Although, for example, the Bayesian approach to inverse modeling allows model errors to be taken into account, in practice the computational costs become very high.

In this study, forward modeling is used to reassess the agreement between measurements and model results given a state of the art description of sources and sinks, to identify the major shortcomings of our understanding of the methane cycle. Second, we investigate how sources and sinks of methane in the model can most efficiently be constrained by measurements. In previous studies [*Fung et al.*, 1991; *Hein et al.*, 1997; *Houweling et al.*, 1999] multiannual data records were used to derive averages or polynomial fits representative of climatological means, trends, and seasonal cycles at observational stations. Preferably, stations were used at large enough distance from the sources, such that measurements represented the scales resolved by the models. Unfortunately, at such stations the fingerprint of sources and sinks has largely been dispersed by atmospheric mixing. In addition, measurements are often smoothed which further reduces the information content of the measurements on sources and sinks. Current global models become increasingly advanced in reproducing smaller temporal and spatial scales. To optimally profit from this model development, more sophisticated methods of using measurements to test these models are needed. To investigate this, first we study which scales can be reproduced by our model, using measurements without any pretreatment by interpolation or smoothing techniques. Different methods of model sampling are tested at background oceanic stations as well as relatively polluted coastal and inland stations. For all model simulations, meteorological input data are used which are representative of the simulated period, to reproduce as accurately as possible the atmospheric conditions at the moment of sampling. When testing the model using limited numbers of samples at relatively polluted sites, representation errors may potentially grow to significant or even dominating proportions. Methods are proposed to minimize these errors or to quantify their potential influence.

This paper is organized as follows: section 2 describes our chemistry transport model, focusing on the representation of the methane cycle. Section 3 describes in situ and flask measurements of methane, used to test the model. To validate large-scale transport properties of the model, simulated and measured latitudinal concentration gradients of SF_6 are compared (section 4). In section 5 the results of methane simulations are presented and methods to reduce representation errors are demonstrated. Further, we focus on the most striking discrepancies between model and measurements, using these methods. Finally, our conclusions are presented in section 6.

2. Model Description

2.1. Chemistry Transport Model

Model simulations presented in this study have been carried out using the global three-dimensional (3-D) Tracer Model 3 (TM3) [*Houweling et al.*, 1998; *Dentener et al.*, 1999]. The geographical resolution applied is 5° in the longitudinal and 3.75° in the latitudinal direction with 19 vertical levels (unless noted). The vertical levels have been defined as terrain following coordinates near the surface, pressure levels in the stratosphere, and a hybrid of the two in between. The horizontal and vertical transport of tracers is based on six hourly mean meteorological fields, including wind, surface pressure, temperature, and humidity, derived from European Centre for Medium-Range Weather Forecasts (ECMWF) reanalyses for the years 1980–1993 and analysis for the years 1994–1996. Each year of model simulation the corresponding meteorological input fields have been used, which applies to all model results presented in this work. The advective transport is calculated using the "slopes scheme" of *Russell and Lerner* [1981]. The subgrid scale convective air mass fluxes are evaluated using the cloud scheme of *Tiedke* [1989], including entrainment and detrainment in updrafts and downdrafts. Turbulent vertical transport is based on stability-dependent vertical diffusion [*Louis*, 1979]. As a test of boundary layer mixing and regional scale transport, ^{222}Rn simulations at various model resolutions have been compared with observations at continental and remote locations [*Dentener et al.*, 1999]. From this study it follows that measured and simulated radon concentrations agree quite well; generally, deviations are <50%. In the present study, results of SF_6 simulation are compared with measurements as a test of large-scale transport (see section 4).

Tropospheric chemistry is represented using a modified version of the Carbon Bond Mechanism 4 [*Houweling et al.*, 1998; *Gery et al.*, 1989], accounting for CH_4/CO and nonmethane hydrocarbon chemistry, including isoprene. Chemical equations are integrated using a Eulerian Backward Iterative scheme, as formulated by *Hertel et al.* [1993]. Emissions of photochemical tracers other than CH_4 are based on the Global Emissions Inventory Activity and Emission Database for Global Atmospheric Research (EDGARV2.0) emission inventories [*Olivier et al.*, 1996; *Guenther et al.*, 1995; *Yienger and Levy*, 1995; *Benkovitz et al.*, 1996]. Wet and dry deposition of soluble and reactive tracers has been described by *Houweling et al.* [1998] and *Ganzeveld et al.* [1998]. Photolysis rates are based on a highly efficient parameterization of the DISSORT radiative transfer code, and a parameterization proposed for wavelength-dependent cross sections and quantum yields accounting for multiple scattering by clouds [*Krol and Van Weele*, 1997; *Landgraf*

and Crutzen, 1998]. O_3 transport from the stratosphere into the upper level of the TM3 model domain is accounted for by containing the ozone concentration in the upper three-model layers, based on ozone concentrations from the climatology by *Fortuin and Kelder* [1998]. Stratospheric HNO_3 is treated similarly, based on UARS-derived O_3/HNO_3 ratios [*Kumer et al.*, 1996; *Bailey et al.*, 1996].

The Chemistry Transport Model (CTM)-derived hydroxyl radical fields have been validated using 1,1,1 trichloroethane (CH_3CCl_3). CH_3CCl_3 can be used to constrain OH, because its sources are relatively accurately known, and the hydroxyl radical
reaction constitutes the most important sink. Surface emissions of CH_3CCl_3 are based on *Midgley* [1989] and *Midgley and McCulloch* [1995]. Stratospheric and oceanic losses of CH_3CCl_3, both small compared with the hydroxyl radical sink, are represented as described by *Houweling et al.* [1998] and *Kanakidou et al.* [1995]. CH_3CCl_3 measurements of the Atmospheric Lifetime Experiment/ Global Atmospheric Gases Experiment network [*Prinn et al.*, 1992, 1994] for 1980–1992 have been compared with model results. More recent data have been omitted since the sources of CH_3CCl_3 have become less certain after implementation of the Montreal Protocol on Substances that Deplete the Ozone Layer. The 1980–1992 ECMWF reanalysis meteorological data were used to simulate the transport of CH_3CCl_3. In addition, for the same period we took variations and trends of emissions and ozone columns into account to compute hydroxyl radical distributions [*Fortuin and Kelder*, 1998; *Lelieveld and Dentener*, 2000],[J. van Aardenne et al., A 1° x 1° resolution dataset of historical anthropogenic trace gase emissions for the period 1890-1990, submitted to *Global Biogeochemical Cycles*, 1999]. From the CH_3CCl_3 simulation a scaling factor is derived, optimizing the agreement between measured and model simulated CH_3CCl_3 as described by *Houweling et al.* [1999]. The computed atmospheric lifetime of CH_3CCl_3, after optimization, ranges from 5.0 years in 1980 to 4.7 years in 1990, within the 4.8 ± 0.3 years calculated by *Prinn et al.* [1995] (unscaled hydroxyl radical fields yield 11% longer lifetimes).

2.2. Methane Simulations

To simulate methane, 4-year model simulations have been performed, of which methane concentrations computed for the final year are compared with measurements only. According to *Hein et al.* [1997] and *Tans* [1997], a spin-up time of 3 years is sufficiently long to avoid a strong influence of the initial CH_4 distribution on the results. To initialize methane, a uniform mixing ratio is prescribed for the whole model domain, derived from results of inverse modeling [*Houweling et al.*, 1999]. When model results are compared with measurements the contribution of the initial methane field to the global mean concentration is eliminated by adjusting the offset in the computed concentrations to background stations (details can be found in figure captions). The CH_3CCl_3 optimized hydroxyl radical fields are prescribed as three-dimensional monthly means. This method yields a tropospheric methane turnover time of 7.8 years, and a tropospheric removal of 509 Tg(CH_4) for 1993.

The sources of methane (roughly representative of 1990) are repeated each year, except for natural wetlands, because dependencies on rainfall and temperature are accounted for according to *Walter* [1998]. The interannual variability of biomass burning and rice paddy emissions are difficult to quantify and have therefore been neglected. For the remaining sources the interannual variability is expected to be small. The observed trend in the global mean methane concentration decreased from 0.6 to 0.2% growth per year [*Dlugokencky et al.*, 1998] over the simulated period (1989–1996), suggesting a more or less stationary global source strength. In absence of indications that a specific source has significantly changed over this relatively short period, we assume that no trend in any of the sources is present. The stratospheric destruction of methane by photolysis and reaction with OH, Cl, and $O(^1D)$ is derived from two-dimensional photochemical model calculations [*Brühl and Crutzen*, 1993], scaled to a global loss of 40 Tg(CH_4) yr^{-1} in agreement with *Crutzen* [1995].

Sources of methane are represented in the model as specified in Table 1. For details of emission distributions and annual totals we refer to the references listed in this table. This

Table 1. Prescribed CH_4 Surface Fluxes

Process	Annual Total	Reference [a]
Anthropogenic Surface Fluxes		
Oil/gas production	51	OL(1,2)
Coal mining	38	OL(1,2)
Waste treatment [b]	73	LE(1),OL(1,2)
Domestic ruminants [c]	93	OL(1,2)
Biomass burning	40	LE(1), OL(2), H91(3), SH(2,3)
Rice agriculture	80	LE(1), M91(2,3)
Other sources [d]	20	OL(1,2)
Natural Surface Fluxes		
Natural wetlands	145	LE(1), BW(2,3)
Termites	20	LE(1), SA(2)
Oceans	15	LE(1), SH(2)
Volcanos	3.5	LA(1), SH(2)
Wild animals	5	LE(1), SH(2)
Soil oxidation	-30	LE(1), AR(2,3)
Total	554	

All fluxes in Tg(CH_4) yr^{-1}.

[a]OL, *Olivier et al.* [1996]; LE, *Lelieveld et al.* [1998]; H91, *Hao et al.* [1991]; M91, *Matthews et al.* [1991]; SA, *Sanderson* [1996]; LA, *Lacroix* [1993]; FU, *Fung et al.* [1991]; BW, *Walter* [1998]; AR, *Ridgwell et al.* [1999]; SH, *Houweling et al.* [1999]; 1, annual and global total; 2, spatial distribution; 3, seasonality (if not specified, a constant source is assumed).

[b]Includes landfills and waste water.

[c]Includes digestion (OL) and waste (LE).

[d]Sum of fossil fuel and domestic biofuel combustion, industrial production of iron, steel, and chemicals.

representation of the sources largely corresponds to the a priori scenario used in the inverse modeling study by *Houweling et al.* [1999], using an older version of the model (TM2) (referred to as SH99 hereinafter). Note that the a posteriori emission fields derived from the SH99 inversion have not been used here since these emission updates to some extent compensate for errors in the transport. For example, part of the a priori to a posteriori emission changes compensate for an overestimate by the model of the latitudinal methane gradient, which could partly be explained by an underestimate of the interhemispheric exchange rate in the model. The updated model, used in the present study (TM3), has an improved representation of interhemispheric transport (see section 4), although the simulated methane gradient remains too large. To further improve this, the geographical distribution of natural wetland emissions has been updated based on process model computations by *Walter* [1998]. This model parameterizes the microbial methane production and consumption in natural wetlands, and the transport through plants and soil as a function of soil and vegetation properties, temperature and hydrological conditions [*Walter et al.*, 1996]. The model has been evaluated and optimized using results of field experiments at a number wetland sites at higher latitudes and a site in the tropics. On the basis of this process model a global emission distribution is obtained with a Northern to Southern Hemisphere emission ratio of 1.38 compared with 1.86 for the distribution applied in SH99 based on *Hein et al.* [1997]. This is explained by a relatively large contribution of tropical wetlands in the estimates by *Walter* [1998].

To improve the representation of microbial methane consumption, sink strengths have been used based on a process model by *Ridgwell et al.* [1999], which, unlike the estimates by *Fung et al.* [1991] applied in SH99, also accounts for seasonal changes. In this model, soil methane oxidation is computed as a function of soil diffusivity and microbial activity. At mid- and high-latitudes, oxidation rates in summer are higher than in winter, which is explained by changes in temperature and soil moisture content. In the tropics, a weak seasonality is found owing to a much smaller seasonal variation in these climatic factors. Finally, as proposed by *Lelieveld et al.* [1998] emissions from industrial waste water have been accounted for, including food and paper industries and oil refineries, estimated at 25 $\pm$10 Tg(CH_4) yr^{-1} [*International Panel on Climate Change*, 1992; *Environmental Protection Agency*, 1994].

3. Measurements

The majority of the measurements used in this study have been performed by the National Oceanic and Atmospheric Administration (NOAA)/ Climate Monitoring and Diagnostics Laboratory (CMDL) cooperative air sampling network [*Dlugokencky et al.*, 1994b]. At each station, duplicate flask samples are taken about once a week and transported to NOAA for analysis. In addition, at Barrow (Alaska, 71°19'N,156°36'W, 11m above sea level (masl)), and Mauna Loa (Hawaii, 19°32'N,155°35'W, 3397 masl) in situ operating gas chromatographs are used, analyzing at a frequency of about 60 samples d^{-1}, which were available to us as hourly averages. The precision of the gas chromatographic analysis of both in situ and flask samples is estimated at 0.2% [*Dlugokencky et al.*, 1994b, 1995]. Measurements "flagged" by NOAA, indicating that the sampled air may have been influenced by local sources, are used in this study. The potential effects of using such samples is discussed in section 5.

In situ measurements at Fraserdale (Canada, 49°53'N, 81°34'W, 250 masl), southeast of the Hudson Bay lowlands, have been carried out by the Atmospheric Environment Service (AES) [*Worthy et al.*, 1998]. Measurements were taken from a 40 m tower at a frequency of 96 d^{-1}. The difference of CH_4 calibration scales used by AES and NOAA/CMDL has been accounted for, on the basis of a recent intercalibration presented in *GLOBALVIEW-CH_4* [1999]. Thus measurements presented in this study are relative to the NOAA/CMDL scale. The precision of the AES gas chromatographic analyses is also 0.2% [*Worthy et al.*, 1998].

4. Interhemispheric Exchange Rate

As indicated in the previous section, interhemispheric gradients give important information on the distribution and strength of CH_4 emissions. Sulfur hexafluoride (SF_6) has been used to test the interhemispheric tracer exchange rate simulated by our CTM. SF_6 is a purely anthropogenic trace gas, emitted mainly from leakages in electronic insulations and switching. In the atmosphere, SF_6 is a virtually inert tracer with an estimated atmospheric residence time of 800 years [*Morris et al.*, 1995]. Annually emitted amounts are determined from the atmospheric budget using global transport models. In our model, the observed trend at Neumayer (8°W,71°S, 42 masl)) [*Maiss and Levin*, 1994; *Maiss et al.*, 1996] is well reproduced using reported emissions by *Levin and Hesshaimer* [1996], multiplied by 0.937 as proposed by *Denning et al.* [1999]. This correction factor is introduced to compensate for differences between the 3-D models used by *Denning et al.* [1999] and the 2-D model used by *Levin and Hesshaimer* [1996]. The global emissions were distributed according to electrical power usage by country and population density [*United Nations*, 1994; *Tobler*, 1995; *Denning et al.*, 1999].

SF_6 has been simulated for the period 1989–1993, of which the final year is used to derive annual mean concentrations, again to avoid effects of errors in the assumed initial hemispheric distribution of SF_6 on the 1993 fields. A comparison between the observed latitudinal gradient, as compiled by *Denning et al.* [1999], and model results is given in Figure 1. These results indicate that the interhemispheric transport rate is quite accurately reproduced by our model. The computed interhemispheric exchange time, as defined by *Prather et al.* [1987], amounts to 0.90 year for 1993. Note that the TM3 results presented by *Denning et al.* [1999] were obtained using European Center/Hamburg-derived meteorological data, as opposed to ECMWF data that have been used here.

To test the sensitivity of the SF_6 test to transport errors, the exchange time in the model has been decreased by 15% by (1) introduction of horizontal diffusion and (2) reducing

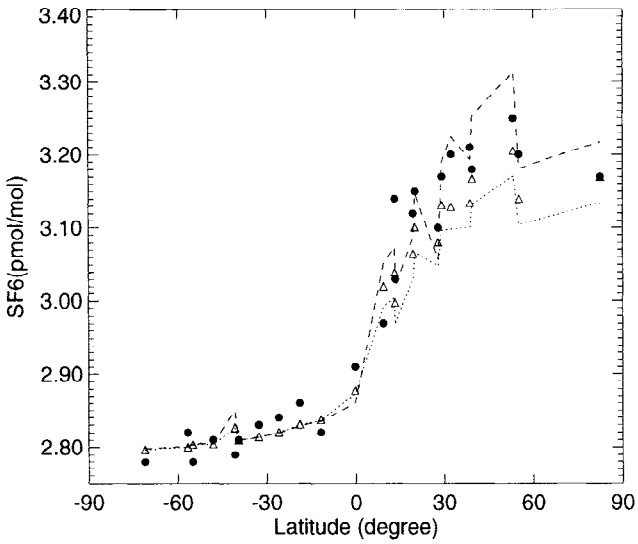

Figure 1. Measured and simulated SF_6 mixing ratios showing the annual mean interhemispheric gradients of SF_6 for 1993. Circles, measurements; triangles, model simulations; dashed line, 15% decreased exchange time by decreased vertical mixing; dotted line, 15% decreased exchange time by increased horizontal diffusion. The offset in the model results has been adjusted to Atlantic Ocean measurements at 40°S.

the vertical mixing by turbulent diffusion and convection. As shown in Figure 1, this leads to a decrease and increase of the simulated SF_6 gradient, respectively, which approximately corresponds to the upper and lower limits of simulated SF_6 gradients that are still in agreement with the measurements. A similar uncertainty is associated with the simulation of transport for the long-lived trace gases CH_3CCl_3 and CH_4. It may seem somewhat illogical that a decreased vertical mixing leads to a decreased exchange time. Although a reduction of vertical mixing leads to an enhanced surface concentration gradient, the difference of SF_6 burden between both hemispheres is less. The increased surface gradient enhances the horizontal tracer exchange at the equator, which explains the decreased exchange time. Note that in our off-line model a reduction of vertical diffusion and convection does not affect the large-scale circulation.

5. Results and Discussion

This section focuses on comparisons between model simulations and measurements at single locations. First, however, we show the ability of the model to reproduce the observed global-scale methane concentration distribution. This provides insight in the extent to which differences between model results and measurements at individual stations are explained by large-scale phenomena. In this section, model results at sites are derived by linear interpolation of the concentrations simulated for the surrounding model grid boxes.

Measured and simulated annual mean latitudinal concentration gradients of methane are presented in Figure 2 (top panel). It shows that the model overestimates the interhemispheric gradient by about 40 nmol/mol (30%), which is a 25% improvement compared to our previous work (SH99). As shown in section 4 at most half of this discrepancy can be explained by transport errors. The changed natural wetland emission distribution and more efficient cross equatorial transport in TM3 resulted in a larger improvement of the simulated methane gradient. However, the updated parameterization of soil oxidation tends to increase the gradient again, owing to an increased contribution of the tropics, as compared with the distribution by *Fung et al.* [1991] we used previously.

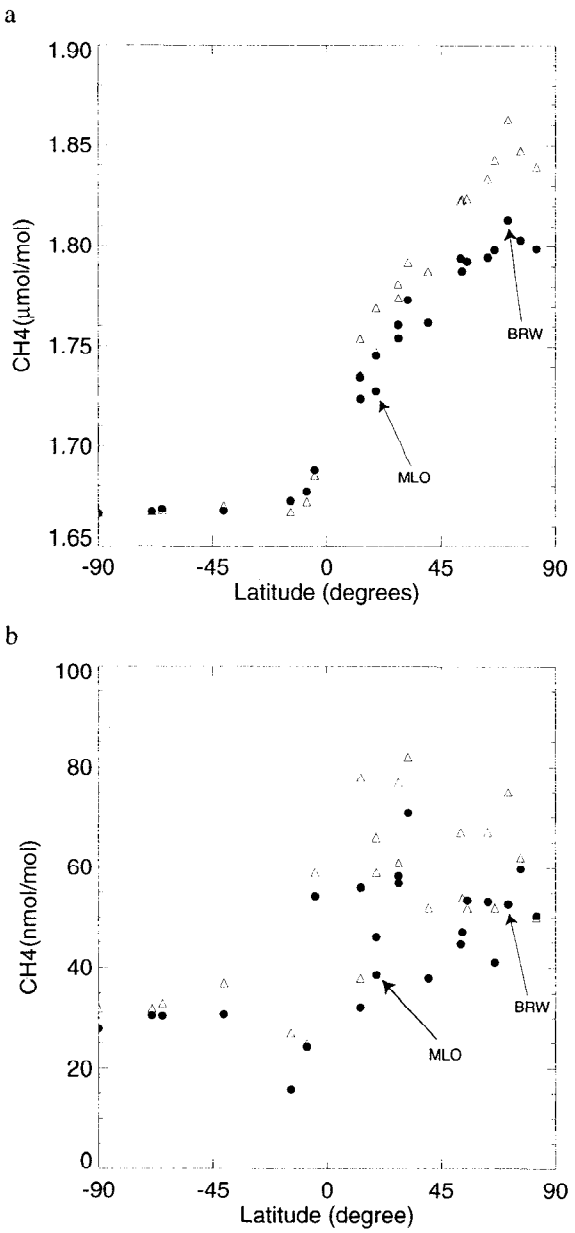

Figure 2. (a) Measured and simulated mixing ratios of CH_4 showing the annual mean interhemispheric gradients of CH_4 for 1993. The offset in the model results has been adjusted to the South Pole (90°S, 25°W 2810 masl). (b) Measured and simulated seasonal cycle amplitudes, estimated from the difference between highest and lowest monthly mean for 1993. Circles represent measurements; and triangles represent model simulations.

The simulated amplitudes of seasonal cycles show a general overestimation compared to observations, particularly in the Northern Hemisphere (Figure 2, bottom panel). This bias points to errors in the balance between sources with distinct seasonal cycles, such as biomass burning, wetland emissions, and the soil and/or hydroxyl radical sink. In the tropics, where the seasonality is partly determined by the movement of the intertropical convergence zone (ITCZ), the overestimated amplitudes may also be related to the overestimated latitudinal methane gradient.

For 1993, a tropospheric average trend of 0.2% is computed, in good correspondence with the observed global averaged increase of 4 nmol $mol^{-1}yr^{-1}$ and global mean mixing ratio of 1715 nmol/mol for this year [*Dlugokencky et al.*, 1998]. Also, we obtain a fair agreement between the observed and simulated annual mean concentration at background stations. As a result, the applied offset adjustments are only small (0.5 and -18.6 nmol/mol for the Southern and Northern Hemisphere, respectively). The fact that both the observed trend and the mean concentration are accurately reproduced by the model indicates that the combination of assumed sources and CH_3CCl_3-calibrated sinks realistically represents the CH_4 budget. It is true that the background level is also related to the applied initial concentration, but a fortunate choice of initial condition in combination with an inaccurately simulated net source/sink would yield an inaccurate trend.

5.1. In situ Measurements

High-frequency in situ measurements at Mauna Loa and Barrow provide useful information about methane concentration variations on different temporal and spatial scales. Although a rigorous analysis of these scales would require many stations, testing the model at Mauna Loa and Barrow is valuable already. This is partly the case because these stations are located in very different environments, representative of well-mixed free tropospheric air (Mauna Loa), and the continental boundary layer, much closer to (possibly even local) sources of methane (Barrow). Model results and in situ measurements at these stations are presented in Figures 3 and 4. At both locations the model has been "sampled" using the same time schedule as for the measurements. This synchronized sampling also explains the straight line segments in these figures when there are no measurements performed.

The Mauna Loa station is located at 3.4 km altitude on the north slope of the Mauna Loa volcano on Hawaii. This geographical location largely determines the daily flow conditions at the station. During daytime, radiative heating of the island induces convective upslope winds transporting air from lower altitudes to the station. After sunset the land–sea circulation reverses and free-tropospheric air is transported to Mauna Loa by a katabatic downslope flow [*Atlas and Ridley*, 1996]. As a result, methane measurements at Mauna Loa show a distinct daily cycle (see Figure 3, e.g. days 110–130) with maxima during daytime and minima during nighttime. Since in the model these up-slope and down-slope winds are not resolved, the variability of the simulated methane concentration on the timescale of a day is underestimated. In the model the concentration difference between sea level and 3.4 km altitude at Hawaii amounts to 22 nmol/mol, which confirms that such local winds may largely explain the diurnal variation of methane at Mauna Loa.

On the timescale of a week the observed variability is quite well reproduced by the model (e.g., days 130–150 and 240–270). The amplitude of the seasonal cycle is slightly overestimated, as can be seen when comparing the means of December–January to July–August. Partly, this is explained by the overestimated interhemispheric gradient since during the July–August period Mauna Loa is relatively frequently influenced by air from the equatorial tropics [*Harris et al.*, 1992], that is from the southern hemispheric "compartment" of the Hadley circulation in this part of the year. Also the seasonality of tropical sources and the hydroxyl radical sink may, however, contribute.

At Barrow the picture is quite different. Periods for which the model performs reasonably (e.g., days 250–300) are alternated by periods where model and measurements do not correlate (e.g., days 60–90). This variable model performance is manifest on different timescales, from reasonable agreement on small scales (e.g., days 200–210) to significant overestimates on the seasonal scale (e.g., days 150–200). The latter is likely related to the representation of arctic natural wetlands, the largest high-latitude source, in particular at relatively high temperatures during summer. On smaller scales, model resolution may become a limiting factor. However, a similar model run on 2.5° x 2.5° resolution did not lead to significant improvements, so that other factors, for example temporal variability of the regional sources, may be more important. In springtime the amplitude of the simulated daily cycle, which peaks before sunrise, is strongly overestimated by the model (see, e.g., the peaks in the model simulations for day 150–170). This suggests an overestimate of local sources, or an underestimate of boundary layer mixing.

5.2. Flask Measurements

A direct comparison of model results and flask measurements is a difficult test for the model. In fact, whether or not the model reproduces single measurements is of limited value since this may largely be accidental. Alternatively, monthly averaged concentrations can be used. As can be deduced from Figures 3 and 4, weekly flask samples are expected to poorly represent monthly concentration distributions, at least at stations that show similar variabilities. As a consequence, an error is introduced when comparing model-derived means, based on concentrations computed at each model time step, to averages derived from flask sampling. As pointed out by *Haas - Laursen et al.* [1997], reducing the frequency of model sampling to the flask sampling frequency does not reduce this error. Rather, a second statistical error is introduced. Sampling synchronization, however, will reduce such errors since we do not intend to estimate the monthly mean concentration, but an average of a set of measurements during a month, of which the individual samples represent the same time.

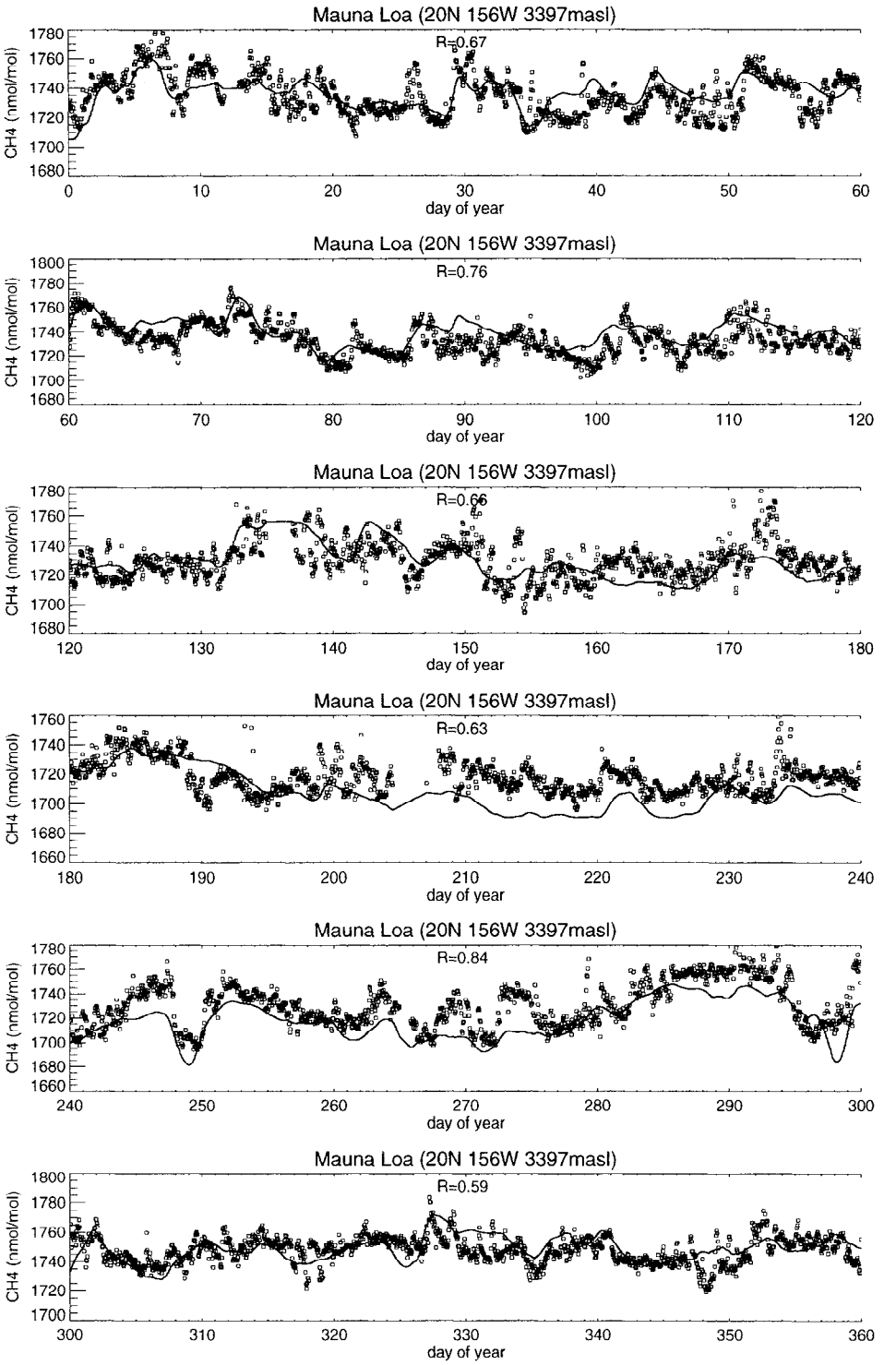

Figure 3. Comparison of in situ measurements at Mauna Loa to model simulations for 1993. Squares, measurements; solid lines, simulations. The offset of the model results has been adjusted to match the annual mean at Mauna Loa. R denotes the correlation coefficient of residual concentrations of model simulations and measurements. Residuals are defined as the difference between daily averages and panel (60 days) averages.

Figure 5 shows the agreement between flask samples (averages of duplicates) and their corresponding simulations at remote to relatively polluted sites. At background stations such as Samoa, Ascension Island, and Midway model and flask measurements agree satisfactorily. A substantial part of the (still substantial) variability is reproduced by the model. At Cape Grim significant differences occur in the first half of the year, which, as we will show later, includes a contribu-

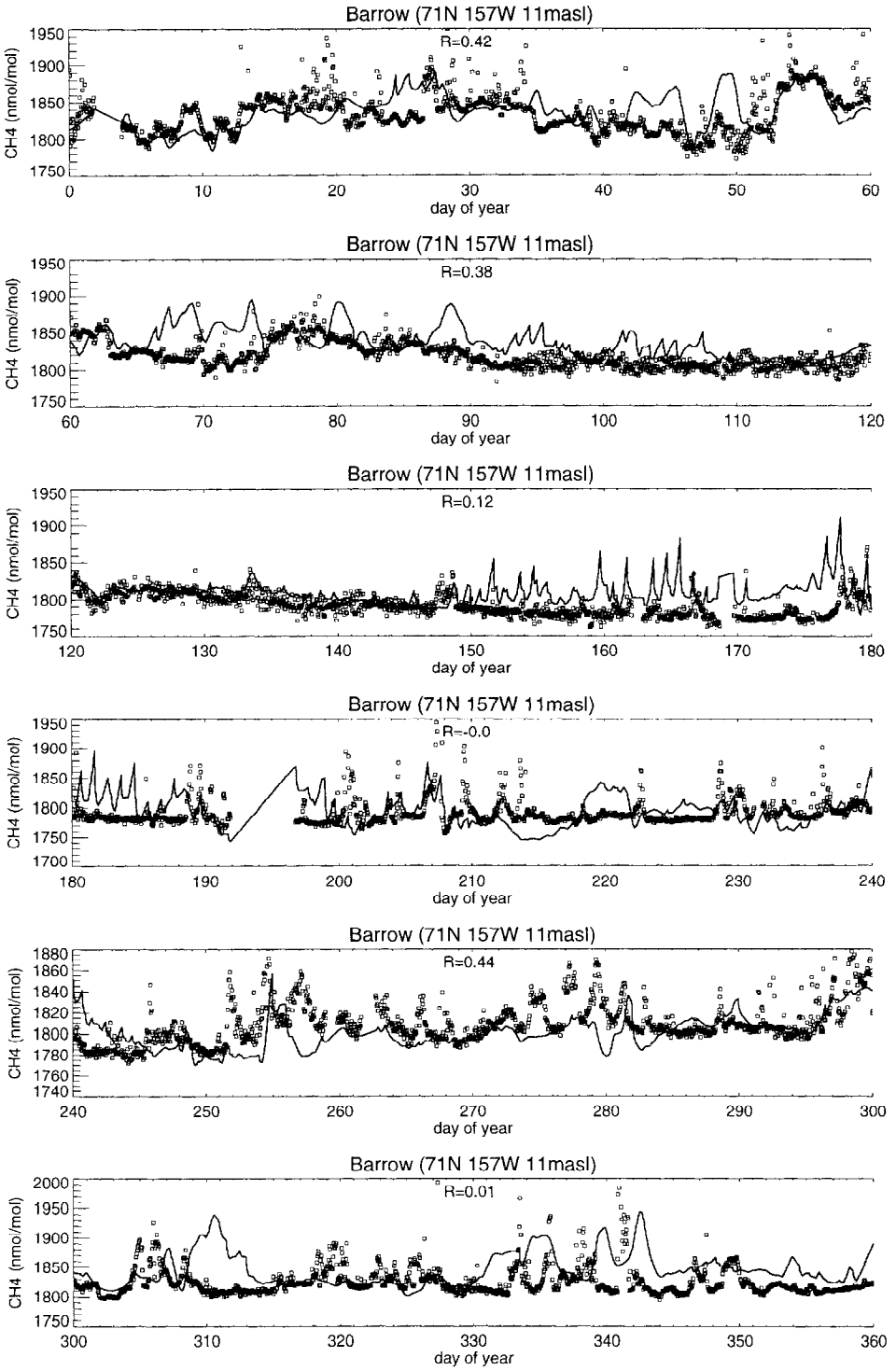

Figure 4. Comparison of in situ measurements at Barrow to model simulations for 1993. Squares, measurements; solid lines, simulations. The offset of the model results has been adjusted such that the measured and modeled baseline concentrations agree. R denotes the correlation coefficient of residual concentrations of model simulations and measurements. Residuals are defined as the difference between daily averages and panel (60 days) averages.

tion by sampling selection at the observatory. At Mace Head and Niwot Ridge the agreement is still fairly good compared with Barrow, indicating that this in situ station is relatively difficult to reproduce by the model. At Tae-Ahn Peninsula there is little agreement between model and measurements particularly during summer, when the observed variability is large as a result of changing wind directions, bringing either clean air from the Pacific or highly polluted air from the Asian continent, where large methane sources are located (see also section 5.4).

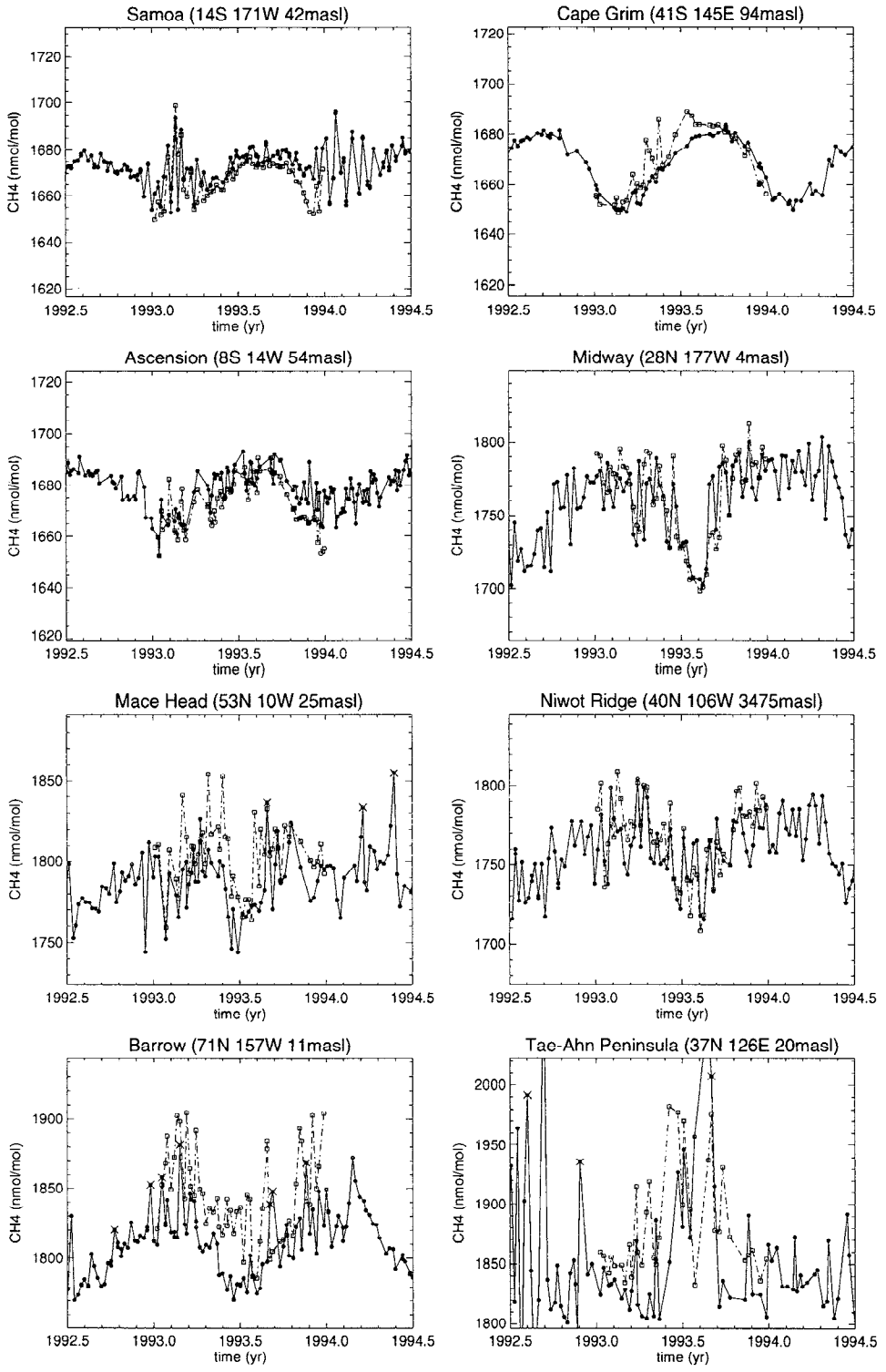

Figure 5. Comparison of flask measurements to model simulations for 1993. Circles, measurements; squares, simulations; asterisks, measurements designated as polluted by NOAA. Measurements exceeding the scale range are designated as polluted by NOAA. The offset of the model results has been adjusted to the annual mean at Midway (for northern hemispheric sites) and the South Pole (for southern hemispheric sites).

To illustrate the effect of synchronized sampling on monthly averages, model-derived high-frequency (model time step) and low frequency (synchronized) means are compared with measurements (Figure 6). At remote stations such as the South Pole (89°59'S, 24°48'W, 2810masl), Samoa (14°15'S, 170°34'W, 42masl) and Syowa (69°00'S, 39°35'E, 11masl) [not shown], differences between simulated high and low frequency monthly means are negligible. This indicates that a frequency of one sample per week is sufficient to quite accurately determine monthly mean concentrations at

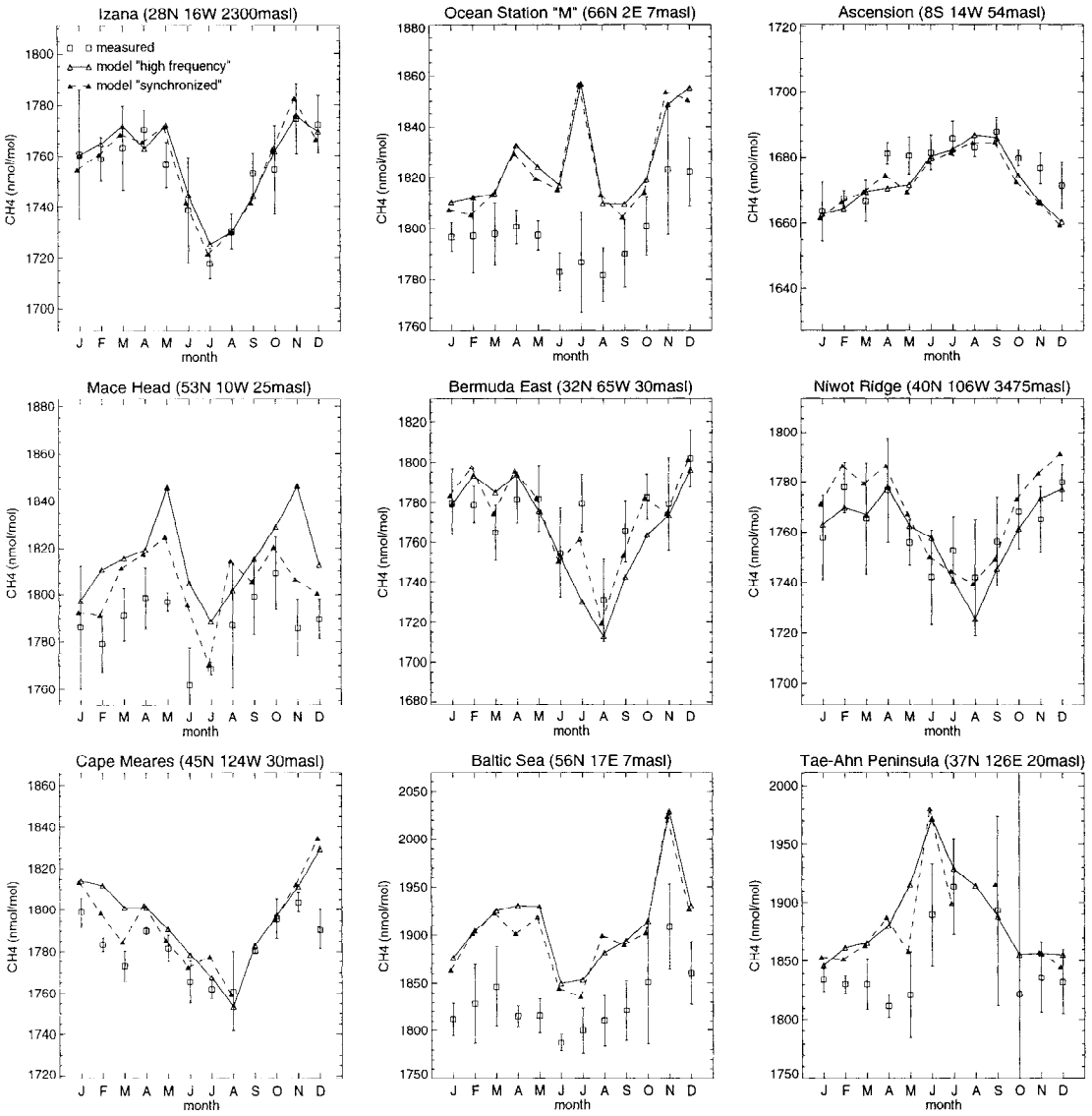

Figure 6. Comparison of monthly means as derived from measurements and model simulations. Squares, measurements with 1σ uncertainties; solid lines, model sampled at each time step; dashed lines, model sampled simultaneous to the measurements. The offset of the model results has been adjusted to the annual mean at Midway (for northern hemispheric sites) and the South Pole (for southern hemispheric sites).

these stations. Similar differences are found at some stations closer to the sources such as Ascension Island, Ocean Station M, and Izana. At stations such as Mace Head, Bermuda, Niwot Ridge, and also at Cape Grim (for the latter see Figure 8), however, significantly different model results are obtained using different sampling frequencies. Here, as expected, weekly samples poorly represent the temporal concentration distribution. Furthermore, the fact that sampling synchronization improves the agreement between model results and measurements means that the model reproduces observed fluctuations of the methane concentration. Effects of sampling frequency on computed monthly averages are also seen at more polluted sites, e.g. at Baltic Sea, Tae-ahn Peninsula and Barrow (for the latter see Figure 8). At these sites, however, synchronized sampling does not significantly improve the agreement with measurements. Here, an important part of the variability is simply not reproduced by the model, as was already seen in the comparisons with in situ data at Barrow.

5.3. Wind Sector Selection

At a number of stations air samples are collected only if the wind direction is from a certain wind sector, with the intention to avoid contamination by local sources and, thus, to extend the scale for which the sampled air is representative. Unless this wind selection is accounted for in the model, this introduces a representation error when comparing these data to model results. For stations such as Cape Grim previous studies on atmospheric CO_2 have shown that these errors cannot be neglected [*Ramonet and Monfray*, 1996; *Law*, 1996]. Synchronized sampling may compensate for this baseline selection, albeit only to a certain extent since the

observed and modeled wind directions may differ. Furthermore, the clean air sector in the model can differ from reality since the continents are represented at a limited resolution. Alternatively, as proposed by *Ramonet and Monfray* [1996], clean air selection can be accounted for in the model by introducing a ^{222}Rn-like diagnostic tracer with an atmospheric turnover time of about a week, and a homogeneous source over the continents only. Air parcels of continental origin are identified by elevated levels of this diagnostic tracer, and samples are excluded whenever this tracer exceeds a certain threshold.

Based on an analysis of ECMWF wind fields, *Haas - Laursen et al.* [1997] concluded that at Cape Grim and Heimaey winds are selected from the southwest and northeast, respectively. Although this analysis was performed for CO_2, the same results apply to CH_4 since both gases are analyzed from the same samples. NOAA reports wind sector selection at Barrow (north to southeast) [*Fergusin and Rosson*, 1992], although this is not confirmed by *Haas - Laursen et al.* [1997].

A threshold concentration of the diagnostic tracer is determined from its concentration distribution at each station. Figure 7 shows these distributions for samples taken at Cape Grim, Heimaey, and Barrow (ranked from low to high ^{222}Rn concentrations). Ideally, the distributions would have two modes, representative of continental and marine air. Then we would choose the threshold in between. In absence of such well-defined modes, the change in slope is used as the transition point of continental and marine air. In this way we derive thresholds of 0.1 (Cape Grim), 0.15 (Heimaey), and 0.35 (Barrow). Measurements of ^{222}Rn [*Whittlestone et al.*, 1996] at Cape Grim and simulated concentrations over the Australian continent [*Dentener et al.*, 1999] confirm that the Cape Grim threshold is quite realistic for the methane observations at this station.

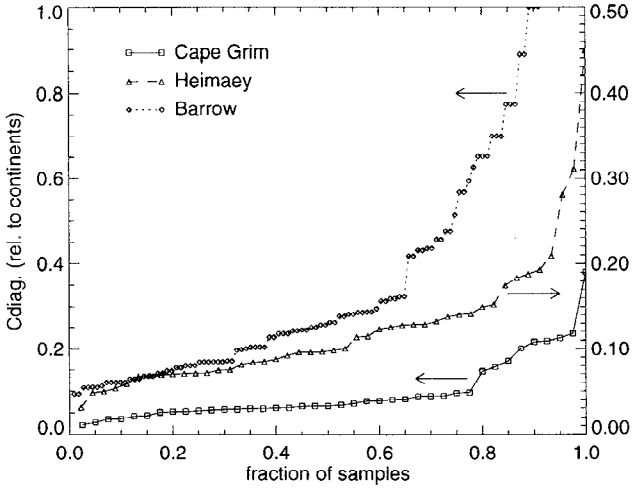

Figure 7. Distributions of diagnostic tracer concentrations (C_{diag}) for wind sector selection. Concentrations are expressed relative to an annual average computed for nearby continents. Arrows indicate the scales (left or right y axis) that correspond to the concentration distributions.

Figure 8 shows the effect of clean air selection at Cape Grim, Heimaey, and Barrow. At Cape Grim, combined sampling synchronization and wind direction selection almost completely explain the overestimation of the simulated monthly means during the first half of the year. At Heimaey the simulated concentration maximum in July, which is absent in the measurements, is significantly reduced when wind direction selection is used. Also at Barrow, clean air sector selection improves the agreement between model and measurements; however, model overestimated concentrations remain in June. Samples that are excluded by clean air sector selection are also not used to compute averages of measurements. As a result, corresponding stations in Figure 8 show differences in measurements and uncertainty ranges. Drastic changes in the computed 1σ uncertainty intervals indicate that these ranges are caused by the small number of measurements.

5.4. Nonlocal Air Selection

Measurements at continental stations have the advantage over remote stations that characteristics of the observed concentration distribution may directly point at sources in a particular region. Their interpretation may, however, be misleading since this region may be smaller than the smallest scale represented by the model ($\sim$ the grid scale). To quantify the potential contribution of subgrid sources, we define a second diagnostic tracer, which is emitted as CH_4 in the four grid boxes closest to a station only. A single tracer can be used for all measurement sites if it is assigned a sufficiently small lifetime, that is, such that the "local" tracer emitted for a particular station does not significantly contribute to its concentration at any other station. On the grid-scale, however, its lifetime should be long enough to mimic methane (approximately inert on these scales). A lifetime of 1 week for the tropics and midlatitudes and 0.5 week at higher latitudes appeared to satisfactorily meet both requirements.

From computed methane and diagnostic tracer concentrations a measure R is derived of the contribution of "subgrid" sources to the simulated concentration at a station i and month m defined as

$$R_{i,m} = \frac{d_{i,m}}{(CH_{4i,m} - CH'_{4m})}, \qquad (1)$$

where d denotes the diagnostic tracer concentration, CH_4 is the methane concentration at the a particular station, and CH_4' is the background concentration at a Pacific site at maximum distance from the continents at the station's latitude. Obviously, the contribution of subgrid sources in the model may differ from the contribution of the corresponding sources in reality. Since it is expected that stations are located at relatively large distances from sources, as compared with their direct surroundings, the real contribution of local sources is not expected to be much larger than indicated by the model-derived R. Whenever $R_{i,m}$ exceeds a certain threshold, the corresponding samples are excluded.

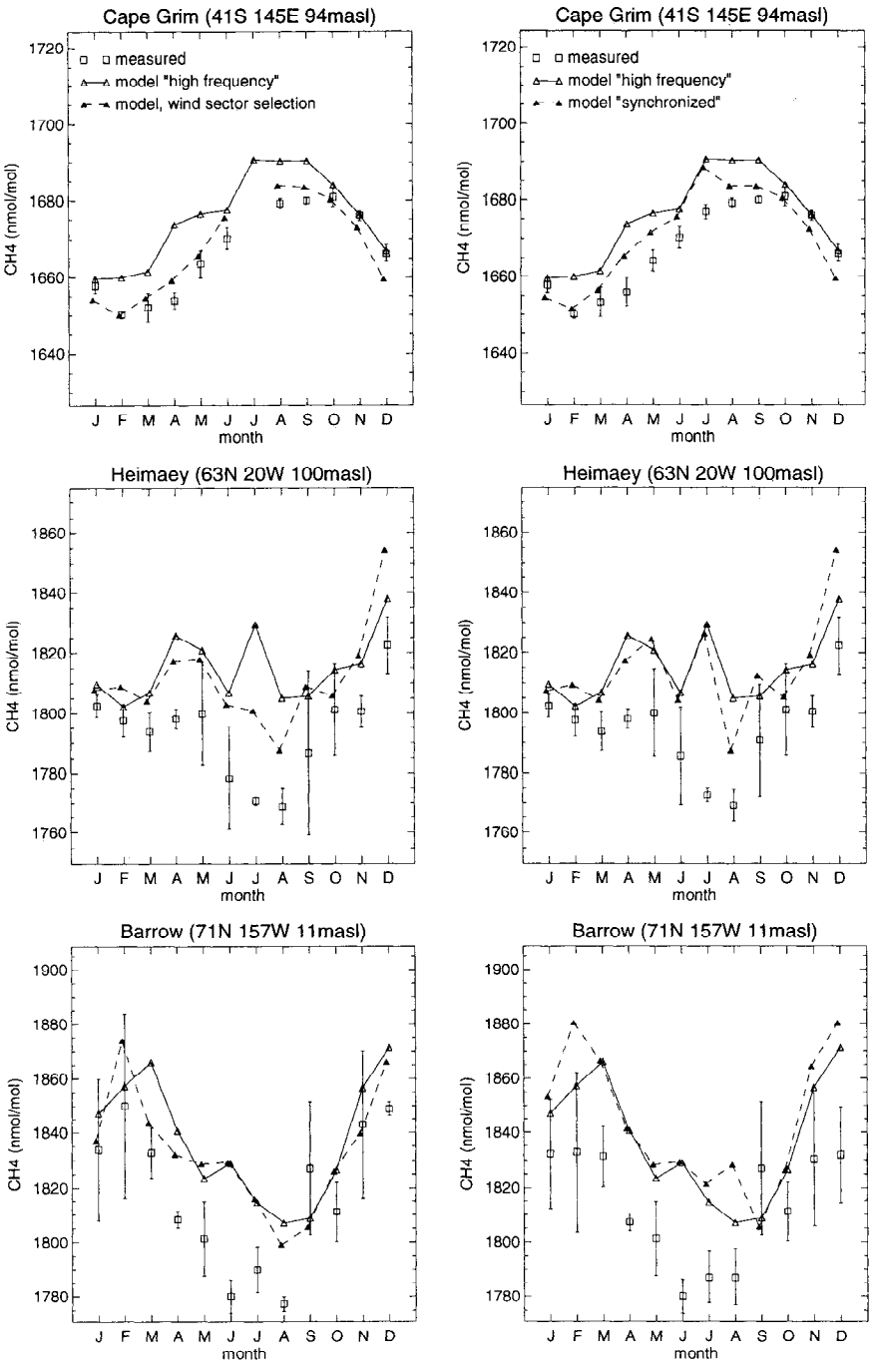

Figure 8. Clean air sector selection. Squares, measurements with 1σ uncertainties; solid lines, model sampled at each time step; dashed lines, model sampled simultaneous to the measurements, (left) with and (right) without clean sector selection. Measurements at Barrow represent flask samples only. The offset in the model is adjusted as in Figure 6.

Figure 9 shows results of this "local influence" filter. In these comparisons a threshold of R=25% is chosen. Since at remote stations the methane concentration may almost be equal to the background reference (CH_4'), here unimportant local sources of methane may already cause a R higher than this threshold. To avoid this, we allowed samples to pass the filter irrespective of R for diagnostic tracer concentrations smaller than 1 nmol/mol. At the Baltic Sea and Barrow, minor effects of filtering locally influenced data can be seen. The main differences between measurements and model computations, however, remain. At Tae-Ahn Peninsula, most of the measurements during summer are identified as locally affected (data gaps in Figure 9 indicate that no sample passed the filter). Averaged over the 1993 samples, the CH_4 concentration at Tae Ahn Peninsula is ~100 nmol mol^{-1} higher than the background ($CH_4 - CH_4$'), with a 37 nmol mol^{-1} contribution of local sources (d). This indicates that comparisons between model and measurements

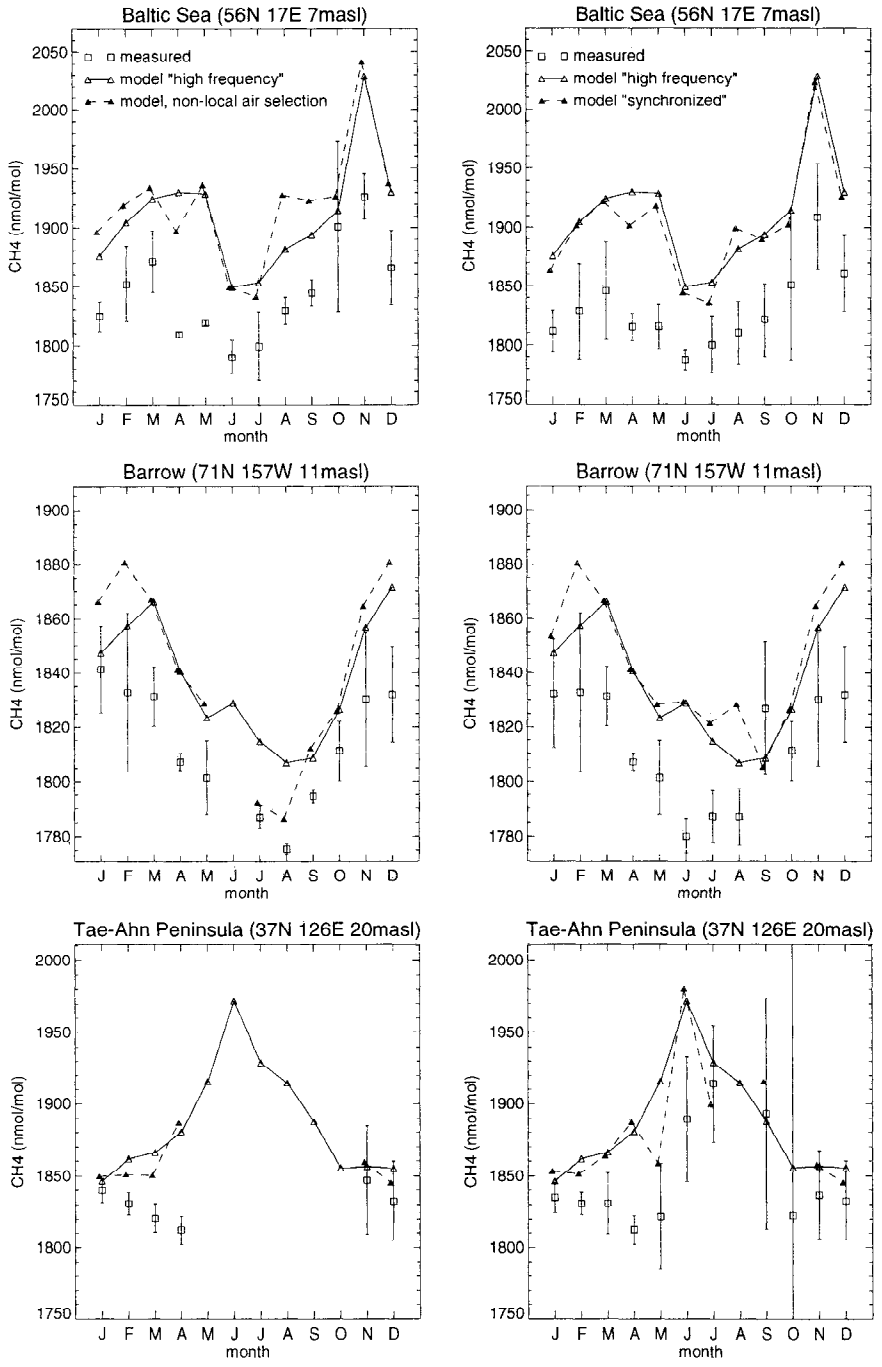

Figure 9. Nonlocal air selection. Squares, measurements with 1σ uncertainties; solid lines, model sampled at each time step; dashed lines, model sampled simultaneous to the measurements, (left) with and (right) without nonlocal air selection. The offset in the model is adjusted as in Figure 6.

at such stations should be treated with care, since differences between model simulations and measurements may largely be explained by sources that are not resolved by the model.

5.5. Influence of Wetland Emissions

The previous sections showed the importance of consistently comparing model results and measurements. However, the question remains what can be learned about atmospheric methane from these comparisons. This subsection focuses on two regions that show the most pronounced differences between model and measurements; the high-latitude stations of the Northern Hemisphere and the South China Sea. These sites are all located in regions with important sources of methane, in particular, natural and agricultural wetlands.

5.5.1. Northern high-latitude wetlands. At Heimaey and Ocean Station M it is shown that the model overestimates methane concentrations in summer (see Figures 6 and

8). In the previous section it was shown that the simulated July maximum at Heimaey may largely be explained by the absence of wind sector selection in the model. However, a similar peak is found at Ocean Station M (see Figure 6) and Ny–Alesund (not shown), where, according to *Haas - Laursen et al.* [1997], no wind sector selection is applied. In contrast, at Barrow such a summertime maximum is absent (Figure 4), although the model significantly overestimates concentrations in June. Figure 10 shows comparisons at three additional stations. The results for Alert and Mould Bay do not confirm that the model overestimates methane concentrations at higher latitudes in summer. Fraserdale, downwind of the Hudson Bay wetlands, strongly points to a model overestimate of wetland emissions. If local contributions >25% are filtered, as explained in the previous section, it appears that the model is not expected to reliably resolve this station in summer. To summarize, although the model has difficulties reproducing the seasonal variation at a number of higher latitude stations of the Northern Hemisphere, this does not unambiguously point to model overestimated emissions.

To determine the potential role of errors in the parameterization of natural wetland emissions, two relatively uncertain parameters have been tested (B. P. Walter, personal communication, 1999). First, the parameter that describes the relative change of methane production rate following a 10 K change of temperature (Q_{10}) has been decreased from 6 to 2. This lower value represents the lower limit of previously reported Q_{10} values, which vary between 1.7 and 16 [*Dunfield et al.*, 1993; *Valentine et al.*, 1994; *Westermann*, 1993].

Secondly, the potential influence of the assumed microtopography of natural wetlands has been assessed. Generally, natural wetlands have a typical complex structure of flooded and dry patches, caused by slight surface elevations (hummocks) or depressions (hollows). The standard parameterization prescribes a uniform water table, determined by the balance between precipitation, evaporation, and runoff. The hydrological conditions of hummocks and hollows are, however, relatively insensitive to the water balance, that is, they remain dry and flooded largely independent of the water supply. As a test it has been assumed that 10% of the northern wetlands (north of 30°N) are water filled throughout the year, whereas 30% are assumed to be hummocks that are so dry that no significant methane production takes place. Global and annual totals have been rescaled to 145 Tg(CH_4) yr^{-1}, in agreement with the standard simulation.

As illustrated in Figure 11, simulated methane concentrations are quite sensitive to the parameterization of natural wetland emissions. A reduction of Q_{10} has a particularly strong influence, significantly improving the agreement between model and measurements at Heimaey and Fraserdale. At Barrow, the model estimate for June improves, but a minimum appears in September which is not seen in the measurements. The importance of Q_{10} is confirmed by a comparison for Alert, although it shows that differences between model and measurements cannot be explained by a uniform reduction of this parameter only. These tests nevertheless indicate that, instead of errors in the absolute magnitude of wetland

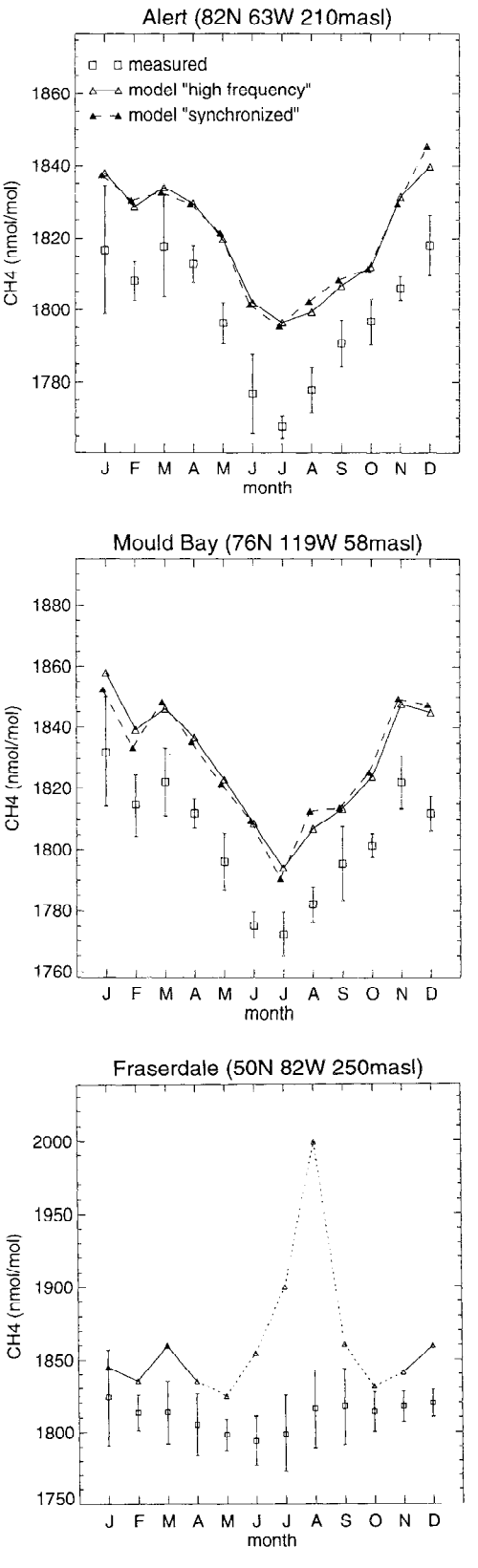

Figure 10. Comparison of monthly means at locations influenced by natural wetland emissions. Squares, measurements with 1σ uncertainties; solid lines, model sampled at each time step; dashed lines, model sampled simultaneous to the measurements; dotted lines, monthly means with a >25% contribution of local sources. The offset in the model is adjusted as in Figure 6.

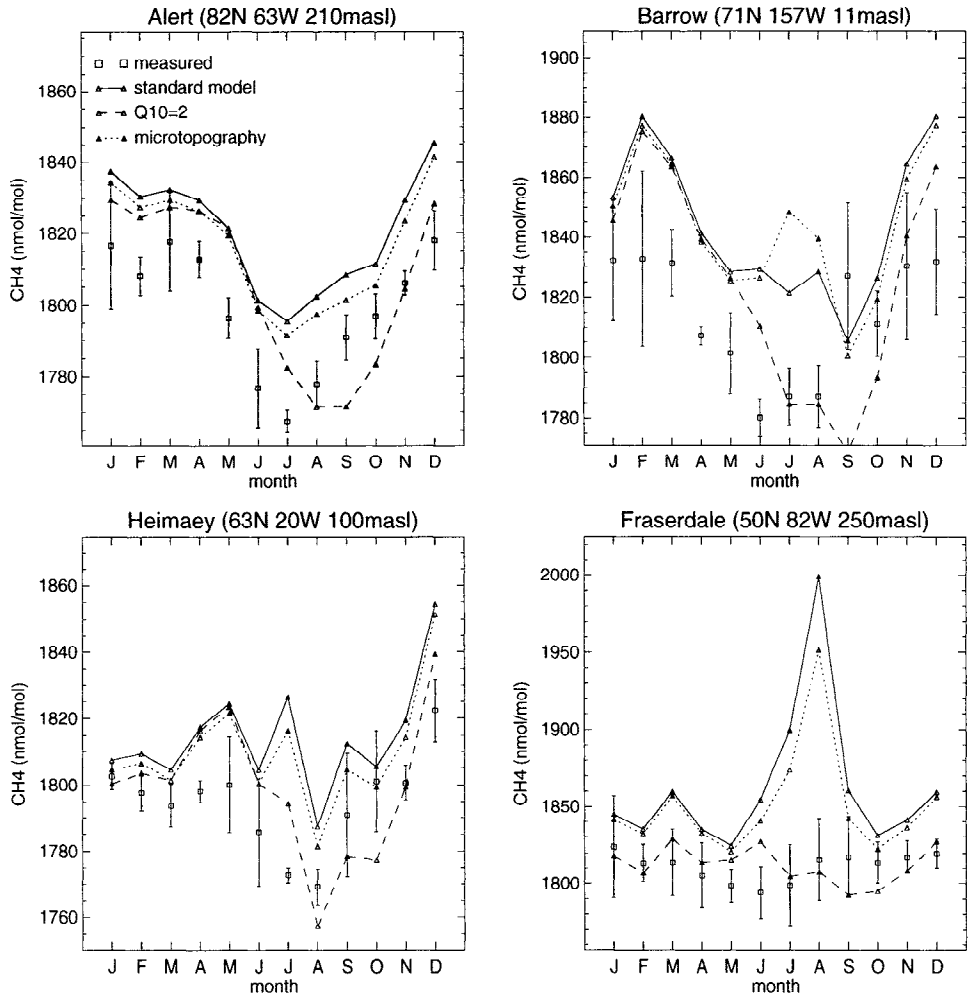

Figure 11. Sensitivity of simulated concentrations to uncertain natural wetland parameters. Squares, measurements with 1σ uncertainties; solid lines, standard simulation; dashed lines, simulation with decreased sensitivity of wetland emissions to temperature changes; dotted lines, simulation accounting for microtopography (see text).

emissions, errors in the distribution and timing of wetland emission may largely explain discrepancies between model and measurements.

5.5.2 South East Asia. To investigate emissions from the Asian continent, measurements at the South China Sea (SCS) in 1992 are used. The samples were taken from cruises from Singapore to Hong Kong at latitudinal intervals of 3° between 3° and 24°N. Ship measurements have the advantage over continental stations, such as Tea-Ahn Peninsula, that the contribution of local sources is negligible. Figure 12 shows simulations and measurements along the South China Sea cruise track. Measurements at Guam, a remote Pacific station at approximately the same latitude as the cruise measurements, are used to correct for the model offset. Generally, these results indicate that the SCS methane concentrations are overestimated by the model. Maximum differences occur in summer, somewhat earlier in the year at the southern (3°N–6°N) compared to the northern locations (15°N–24°N). Although differences between high- and low-frequency sampling of the model are sometimes quite large, this does not alter the general picture. The seasonal pattern is explained by prevailing winds from the continent in winter, as opposed to the summer monsoon, when air from the tropical Pacific is transported over Indonesia to the South China Sea. Although continental sources such as rice paddies are stronger during summer, their influence is masked by a larger supply of background air.

To quantify the contribution of different source regions to the methane concentrations as observed over the South China Sea, marked tracer simulations were performed. For this purpose, four source regions are defined (see Figure 13). In the model, methane emissions from each region are represented by a different marked tracer. Except for their sources, all marked tracers are treated as methane in a standard simulation.

Results of this marked tracer simulation are presented in Figure 14. To highlight the most relevant information, only regions with the most important contributions have been included. At SCS 3°N, as expected, the Indonesian contribution (region *D*) is relatively large since these measurements

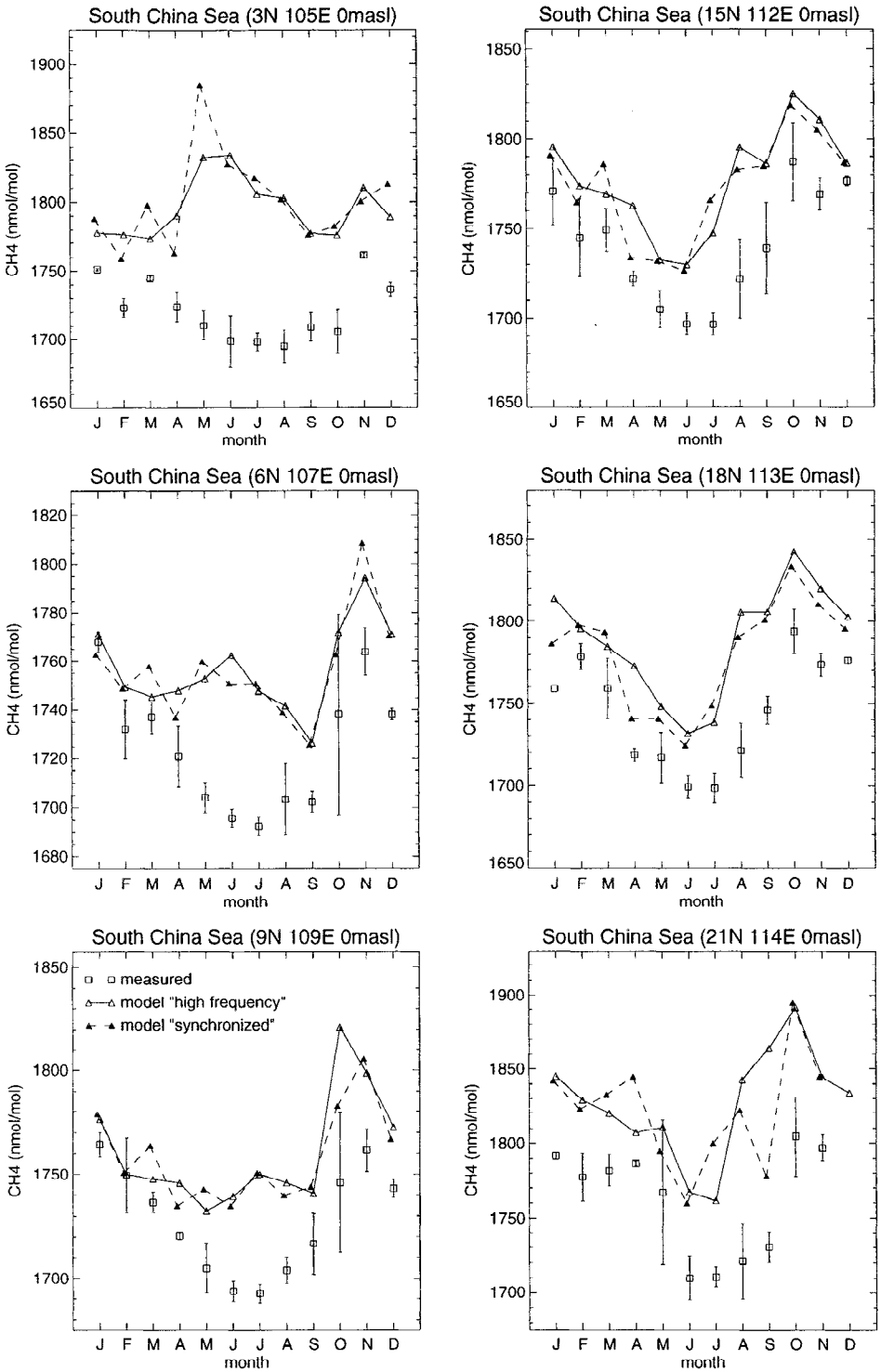

Figure 12. Comparison of model and measurements at the South China Sea for 1992. Squares, measurements with 1σ uncertainties; solid lines, model sampled at each time step; dashed lines, model sampled simultaneous to the measurements (no clean air selection). The offset in the model is adjusted such that the measured and modeled annual means agree at Guam (13°N, 145°E, 2 masl).

are within approximately 300 km north of Singapore. More to the north, the contribution of region *D* decreases and emissions from region *B*, including countries such as Thailand, Laos, and Vietnam, gain importance. Further northward the contribution of this region again decreases and China (region *A*) becomes more important. Thus the region contributing strongest to the simulated concentrations changes with the sampling location, whereas the model overestimates methane over the entire South China Sea. It follows that the model overestimated concentrations are not explained

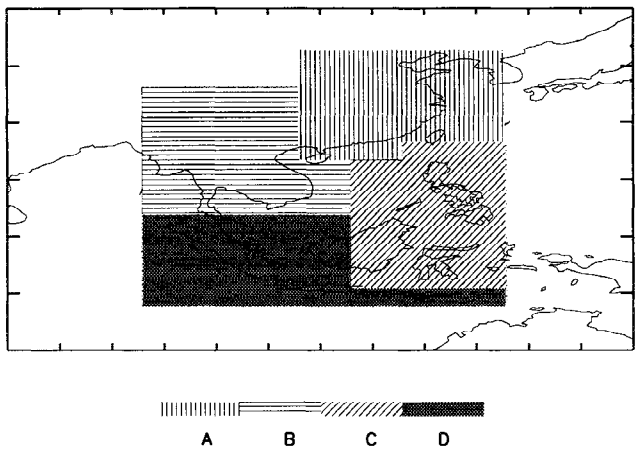

Figure 13. Definition of source regions affecting South China Sea samples. The lower-left corner of region *D* is at 92°30'E, 11°15'S; the upper-right corner of region *A* is at 127°30'E, 41°15'N.

by emissions from a single region, but rather have contributions from regions *A*, *B*, and *D*, with less contribution from the Philippine region *C*. Although the integrated emissions from all four regions largely explain the observed concentration variations, an important part of the seasonal cycle is explained by sources at larger distance. It follows that methane simulations pertaining to southeast Asia using regional models, require that a quite large model domain is accounted for. Therefore, preferably, regional models should be nested within global models.

To relate differences between model and measurements to particular source processes rather than regions, additional simulations have been carried out in which particular sources are marked (emitted from all regions). Figure 15 shows a large contribution by natural wetland emissions for SCS 3°N and 6°N, most likely related to the natural wetlands of Sumatra. Further north, rice agriculture gains importance, particularly in summer, whereas the sum of other sources, for example, ruminants, fossil fuel, and waste treatment, becomes increasingly important in winter. Generally, the sum of rice paddy and natural wetland emissions contributes more than 50% to methane from Southeast Asian sources, notably when the differences between simulated concentrations and measurements are largest. This indicates that the overestimated concentrations at South China Sea are most likely related to a combination of these wetland sources.

The advantage of using 1992 for the comparisons at South China Sea is the relatively large number of samples that were taken during these particular ship cruises. This year cannot be considered as representative of a larger period, however, since there are indications that methane sources and sinks were influenced by the Mount Pinatubo eruption of June 15, 1991 [*Dlugokencky et al.*, 1994a]. It has been suggested that wetland emissions may have been reduced as a result of changed temperature and precipitation patterns caused by the Mount Pinatubo effluents [*Dlugokencky et al.*, 1996; *Hogan and Harris*, 1994]. To examine the possible influence of Mount Pinatubo, we repeated our model runs for the years 1994 and 1996. As an additional test, we increased the model resolution to 2.5° x 2.5° for 1996. The results of these runs (see Figure 16) indicate that the differences between model and measurements are indeed relatively large in 1992 but cannot be explained by the Mount Pinatubo effect alone.

6. Summary and Conclusions

We presented simulations of tropospheric methane using a CTM and parameterized sources and sinks based on the most recently available information. Measurements obtained by high-frequency (60 d^{-1}) in situ and low-frequency (weekly) flask sampling have been used to evaluate the model and to identify shortcomings. For background stations, such as Ascension Island, Guam, and Midway, the agreement is satisfactory. At Mauna Loa, where in situ measurements are available, a substantial part of the observed short-term ($\sim$ week) variability is reproduced by the model, indicating that large-scale transport is represented well by the model. Except for a 30% overestimate of the interhemispheric (pole-to-pole) concentration gradient and a 25% overestimate of the amplitude of seasonal cycles in the Northern Hemisphere, the representation of sources and sinks largely explains observed concentrations at background stations. Because of the low variability at these stations, monthly mean concentrations can be derived from weekly samples with reasonable accuracy. Differences between simulated monthly means derived from high- and low-frequency sampling of the model at remote stations, such as South Pole, and Syowa, are well within the measurement accuracy.

Model simulations indicate that with decreasing distance to the sources, differences between high- and low-frequency sampling increase, up to 20–30 nmol/mol at Barrow and Mace Head, owing to increased variability on shorter timescales. At stations such as Niwot Ridge, Bermuda East, and Mace Head, the agreement between model and measurements is significantly improved when synchronized sampling is applied, that is, when the model is sampled at the same time and location as the measurements, instead of sampling at each model time step. At even shorter distances to the sources, at Tae Ahn Peninsula, Baltic Sea, and Barrow, sampling synchronization does not lead to significant improvements since other factors, in particular the limited model resolution, become dominant.

For coastal observatories that apply clean sector selective sampling, for example, at Barrow, Cape Grim, and Heimaey, the comparability of measured and modeled monthly means can further be improved by baseline selection in the model. As suggested by *Ramonet and Monfray* [1996], this can be achieved by simulating a diagnostic tracer that marks continental air and by excluding methane samples whenever this tracer concentration exceeds a certain threshold. As previously shown for CO_2, also for CH_4, discrepancies between simulations and measurements at Cape Grim can largely be attributed to sampling selection. Similar effects are shown at Heimaey, Iceland. We showed that from the concentration

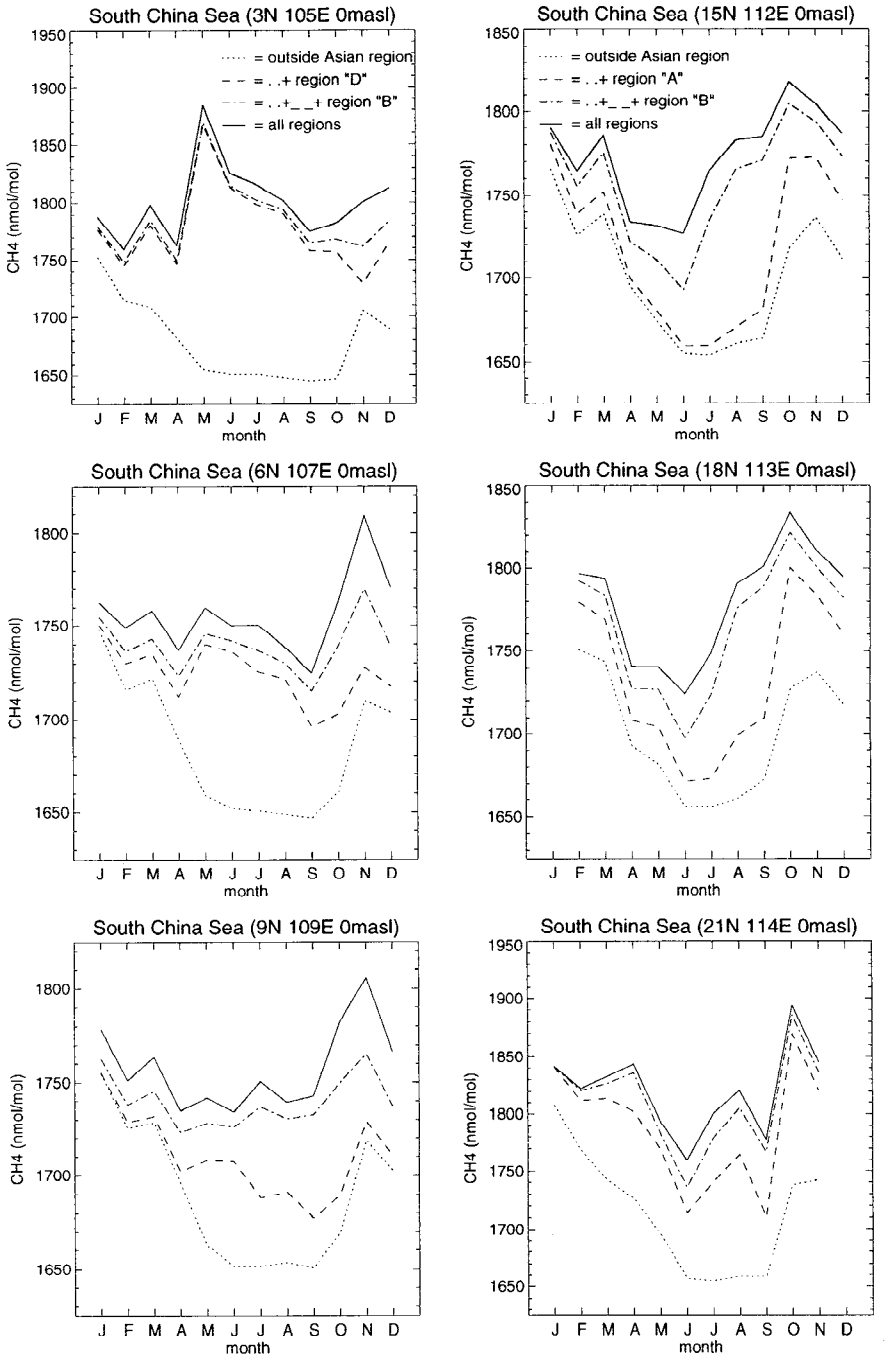

Figure 14. Contribution of specified source regions (see Figure 13) to the simulated methane concentrations at South China Sea. Solid lines, all sources included; dotted lines, all sources except those of the specified source regions; dashed lines, dotted lines plus sources from (left) region D or (right) region A; dashed-dotted, dashed lines plus sources of region B.

distribution of the diagnostic tracer a threshold value can be derived, discriminating between "marine" and "continental" air. This threshold may, however, lead to a different degree of clean air selection in the model as in the measurements. If, in addition, the ^{222}Rn concentration is known at the moment of sampling this can be used to verify this threshold. Generally, we feel that the interpretation of comparisons between measured and model-derived methane would benefit from simultaneous measurements of ^{222}Rn, to discriminate marine and continental air, and, for example, SF_6 to discriminate air influenced by industrial and biogenic sources.

The usefulness of continental observations is limited by processes on smaller scales than represented by the model. To quantify their potential effects, a method is proposed in which the contribution of local grid boxes to the simulated concentration is used as a proxy of "subgrid" sources. Al-

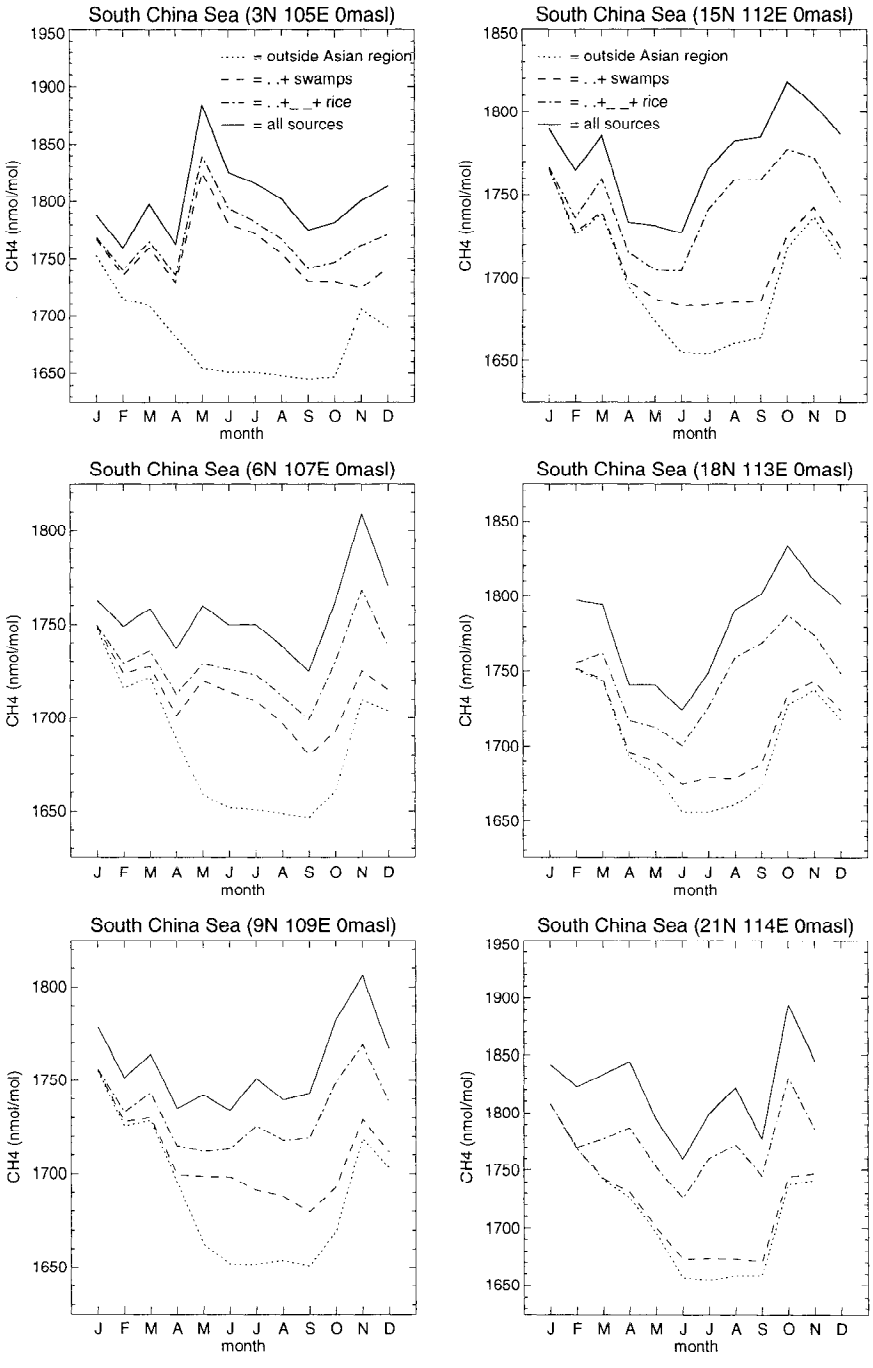

Figure 15. Contribution of wetland emissions from all specified source regions (see Figure 13) to the simulated methane concentrations at South China Sea. Solid lines, all sources included; dotted lines, sources outside the selected domain only; dashed lines, dotted lines plus natural wetland emissions in the selected domain; dashed-dotted, dashed lines plus rice paddy emissions in the selected domain.

though local effects cannot be filtered from the results, it enables assessment of the usefulness of a particular station for testing the model, as illustrated for Barrow, Baltic Sea, and Tae Ahn Peninsula. This procedure indicates that for the present model resolution (3.75°x5°) the Korean station is of limited use.

After screening comparisons of model and measurements for representation errors, unexplained disagreements remain at a number of stations, pointing to shortcomings in the model. The model has difficulties reproducing seasonal variations at stations at higher latitudes of the Northern Hemisphere. Comparisons at Heimaey, Ocean Station M, Barrow, and Fraserdale suggest overestimated natural wetland emissions, which is not confirmed, however, at Alert and Mould Bay. In addition, representation errors related to wind direction selection and subgrid sources may largely explain dif-

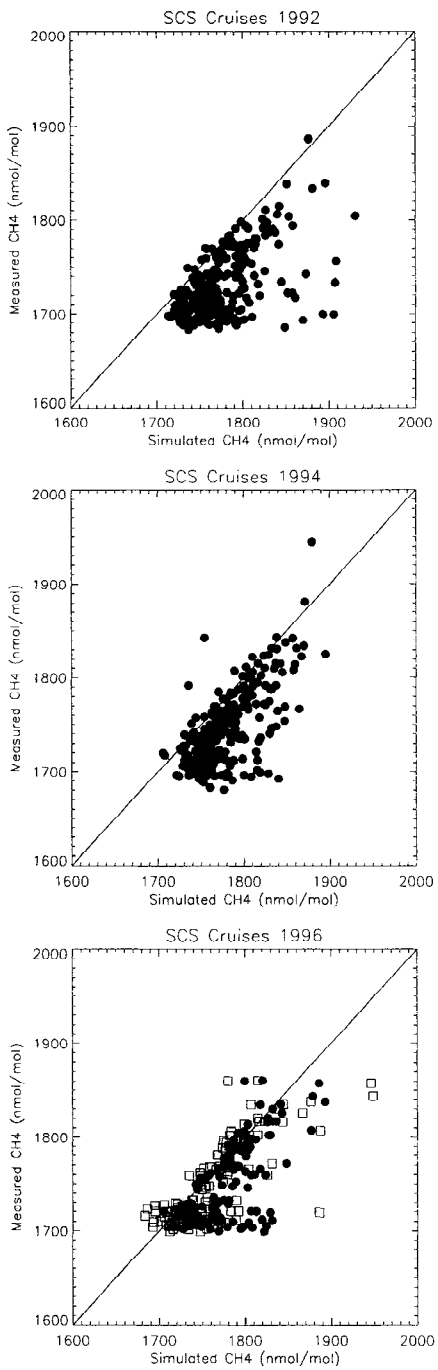

Figure 16. Compilation of measurements and model calculations for all South China Sea cruises. Circles are based on a simulation at 4° x 5° resolution, and squares are based on a simulation at 2.5° x 2.5° degree resolution (1996 only).

ferences between model and measurements at Heimaey and Fraserdale, respectively. To examine the potential role of natural wetland emissions, sensitivity simulations have been performed in which the temperature dependence of wetland methane production and the wetland microtopography were tested. Model simulations indicate that seasonal cycles at Alert, Barrow, Fraserdale, and Heimaey are highly sensitive to these parameters, which could potentially explain much of the discrepancies between model and measurements. This high sensitivity suggests that uncertain process model parameters could be further constrained by inverse modeling.

We further focused on a number of locations in the Southeast Asian region. Three years of measurements indicate that emissions over this continent may have been overestimated. Results of marked tracer simulations, in which methane from different sources and regions is distinguished, point to natural wetland emissions from Sumatra and Chinese rice paddies as likely candidates. Recent estimates on the basis of inverse modeling (SH99) and up-scaling [*Huang et al.*, 1997; *Denier van der Gon*, 2000] point in the same direction.

We conclude that by applying methods to compensate for representation errors, significant improvements in the comparison between model results and measurements can be achieved. Differences of these "screened" modeled concentrations and measurements are a better indication for discrepancies in, for example, emission distributions. The same methods can in principal be applied in inverse modeling, for example, to define a suitable set of measurements or to assess the uncertainties associated with comparisons of measurements and model simulations. This will be the aim of future work.

Acknowledgments. We thank M. Heimann (MPI for Biogeochemistry) and T. Kaminski (MPI for Meteorology) for useful discussions. Further, helpful comments and suggestions were provided by two anonymous reviewers. This work has been supported by the Dutch Global Change program, NOP project 951 202.

References

Atlas, E. L., and B. A. Ridley, The Mauna Loa Observatory Photochemistry Experiment: Introduction, *J. Geophys. Res.*, *101*, 14,531–14,541, 1996.

Bailey, P. L., et al., Comparison of cryogenic limb array etalon spectrometer (CLAES) ozone observations with correlative measurements, *J. Geophys. Res.*, *101*, 9737–9756, 1996.

Benkovitz, C. M., M. T. Scholtz, J. Pacyna, L. Tarrason, J. Dignon, E. C. Voldener, P. A. Spiro, J. A. Logan, and T. E. Graedel, Global gridded inventories of anthropogenic emissions of sulfur and nitrogen, *J. Geophys. Res.*, *101*, 29,239–29,253, 1996.

Brown, M., Deduction of fluxes of source gases using an objective inversion algorithm and a chemical transport model, *J. Geophys. Res.*, *98*, 12,639–12,660, 1993.

Brühl, C., and P. J. Crutzen, MPIC two-dimensional model, *NASA Ref. Publ.*, *1292*, pp. 103–104, 1993.

Crutzen, P. J., The role of methane in atmospheric chemistry and climate, in *Ruminant Physiology: Digestion, Metabolism, Growth and Reproduction: Proceedings of the Eighth International Symposium on Ruminant Physiology*, edited by W. V. Engelhardt, S. Leonhardt-Marek, G. Breves, and D. Giesecke, pp. 291–315, Ferdinant Enke Verlag, Stuttgart, Germany, 1995.

Crutzen, P. J., and P. H. Zimmerman, The changing chemistry of the troposphere, *Tellus*, *43A/B*, 136–151, 1991.

Denier van der Gon, H. A. C., Changes in CH_4 emissions from rice fields from 1960 to the 1990s, 1, Impacts of modern rice technology, *Global Biogeochem. Cycles*, in press, 2000.

Denning, A. S., et al., Three-dimensional transport and concentration of SF_6: A model intercomparison study (Transcom 2), *Tellus, Ser. B*, *51*, 266–297, 1999.

Dentener, F. J., J. Feichter, and A. Jeuken, Simulation of the transport of ^{222}Rn using on-line and off-line global models at different horizontal resolutions: A detailed comparison with measurements, *Tellus, Ser. B*, *51*, 573–602, 1999.

Dlugokencky, E. J., K. A. Masarie, P. M. Lang, P. P. Tans, and E. G. Nisbet, A dramatic decrease in the growth rate of atmospheric methane in the Northern Hemisphere during 1992, *Geophys. Res. Lett.*, *21*, 45–48, 1994a.

Dlugokencky, E. J., L. P. Steele, P. M. Lang, and K. A. Masarie, The growth rate and distribution of atmospheric methane, *J. Geophys. Res.*, *99*, 17,021–17,043, 1994b.

Dlugokencky, E. J., L. P. Steele, P. M. Lang, and K. A. Masarie, Atmospheric methane at Mauna Loa and Barrow observatories: Presentation and analysis of in situ measurements, *J. Geophys. Res.*, *100*, 23,103–23,113, 1995.

Dlugokencky, E. J., E. G. Dutton, P. C. Novelli, and K. A. Masarie, Changes in CH_4 and CO growth rates after the eruption of Mt. Pinatubo and their link with changes in tropical tropospheric UV flux, *Geophys. Res. Lett.*, *23*, 2761–2764, 1996.

Dlugokencky, E. J., K. A. Masarie, P. M. Lang, and P. P. Tans, Continuing decline in the growth rate of the atmospheric methane burden, *Nature*, *393*, 447–450, 1998.

Dunfield, P., R. Knowles, R. Dumont, and T. R. Moore, Methane production and consumption in temperate and subarctic peat soils: Response to temperature and soil pH, *Soil Biol. Biochem.*, *25*, 321–326, 1993.

Environmental Protection Agency, International anthropogenic methane emissions: Estimates for 1990, *Rep. EPA 230-R-94-010*, edited by J. Adler, Washington, D. C., 1994.

Fergusin, E. E., and R. M. Rosson, Climate monitoring and diagnostics laboratory, *in Summary Report 1991, CMDL Rep. 20*, U. S. Dep. of Commer., Washington, D. C., 1992.

Fortuin, J. P. F., and H. Kelder, An ozone climatology based on ozonesonde and satellite measurements, *J. Geophys. Res.*, *103*, 31,709–31,734, 1998.

Fung, I., J. John, J. Lerner, E. Matthews, M. Prather, L. P. Steele, and P. J. Fraser, Three-dimensional model synthesis of the global methane cycle, *J. Geophys. Res.*, *96*, 13,033–13,065, 1991.

Ganzeveld, L., J. Lelieveld, and G. J. Roelofs, A dry deposition parameterization for sulfur oxides in a chemistry and general circulation model, *J. Geophys. Res.*, *103*, 5679–5694, 1998.

Gery, M. W., G. Z. Whitten, J. P. Killus, and M. C. Dodge, A photochemical kinetics mechanism for urban and regional scale computer modeling, *J. Geophys. Res.*, *94*, 925–956, 1989.

GLOBALVIEW-CH_4, Cooperative atmospheric data integration project: Methane, *CD-ROM*, NOAA Clim. Monit. and Diagnostics Lab., Boulder, Colo., 1999.

Guenther, A., et al., A global model of natural volatile organic compound emissions, *J. Geophys. Res.*, *100*, 8873–8892, 1995.

Haas - Laursen, D. E., D. E. Hartley, and T. J. Conway, Consistent sampling methods for comparing models to CO_2 flask data, *J. Geophys. Res.*, *102*, 19,059–19,071, 1997.

Hao, W. M., M. H. Liu, and P. J. Crutzen, Estimates of the annual and regional releases of CO_2 and other trace gases to the atmosphere from fires in the tropics based on the FAO statistics for the period 1975-1980, in *Fire in the Tropical Biota*, edited by J. Goldhammer, pp. 440–462, Springer-Verlag, New York, 1991.

Harris, J. M., P. P. Tans, E. J. Dlugokencky, K. A. Masarie, P. M. Lang, S. Whittlestone, and L. P. Steele, Variations in atmospheric methane at Mauna Loa Observatory related to long-range transport, *J. Geophys. Res.*, *97*, 6003–6010, 1992.

Hein, R., P. J. Crutzen, and M. Heimann, An inverse modeling approach to investigate the global atmospheric methane cycle, *Global Biogeochem. Cycles*, *11*, 43–76, 1997.

Hertel, O., R. Berkowicz, J. Christensen, and O. Hov, Test of two numerical schemes for use in atmospheric transport-chemistry models, *Atmos. Environ., Part A*, *27*, 2591–2611, 1993.

Hogan, K. B., and R. C. Harris, Comment on "A decrease in the growth rate of atmospheric methane in the Northern Hemisphere during 1992" by E. J. Dlugokencky et al., *Geophys. Res. Lett.*, *21*, 2445–2446, 1994.

Houweling, S., F. J. Dentener, and J. Lelieveld, The impact of nonmethane hydrocarbon compounds on tropospheric photochemistry, *J. Geophys. Res.*, *103*, 10,673–10,696, 1998.

Houweling, S., T. Kaminski, F. J. Dentener, J. Lelieveld, and M. Heimann, Inverse modelling of methane sources and sinks using the adjoint of a global transport model, *J. Geophys. Res.*, *104*, 26,137–26,160, 1999.

Huang, Y., R. L. Sass, and F. M. Fisher, Methane emissions from Texas rice paddy soils, 1, Quantitative multi-year dependence of CH_4 emissions on soil, cultivar and grain yield, *Global Change Biol.*, *3*, 479–489, 1997.

International Panel on Climate Change, Climate change 1992: The supplementary report to the IPCC Scientific Assessment, in *Climate Change 1994*, edited by J. T. Houghton, B. A. Callander, and S. K. Varney, Cambridge Univ. Press, New York, 1992.

Kanakidou, M., F. J. Dentener, and P. J. Crutzen, A global three-dimensional study of the fate of HCFCs and HFC-134a in the troposphere, *J. Geophys. Res.*, *100*, 18,781–18,802, 1995.

Kandlikar, M., Bayesian inversion for reconciling uncertainties in global mass balances, *Tellus*, *49B*, 123–135, 1997.

Krol, M., and M. Van Weele, Implications of variation of photodissociation rates for global atmospheric chemistry, *Atmos. Environ.*, *31*, 1257–1273, 1997.

Krol, M., P. J. van Leeuwen, and J. Lelieveld, Global OH trend inferred from methylchloroform measurements, *J. Geophys. Res.*, *103*, 10,697–10,711, 1998.

Kumer, J. B., et al., Comparison of correlative data with HNO_3 version 7 from the CLAES instrument deployed on the NASA Upper Atmosphere Research Sattelite, *J. Geophys. Res.*, *101*, 9621–9656, 1996.

Lacroix, A. V., Unaccounted-for sources of fossil and isotopically-enriched methane and their contribution to the emissions inventory: A review and synthesis, *Chemosphere*, *26*, 507–557, 1993.

Landgraf, I., and P. J. Crutzen, An efficient method for online calculations of photolysis and heating rates, *J. Atmos. Sci.*, *55*, 863–878, 1998.

Law, R., The selection of model-generated CO_2 data: A case study with seasonal biospheric sources, *Tellus*, *48B*, 474–486, 1996.

Lelieveld, J., and F. J. Dentener, What controls tropospheric ozone?, *J. Geophys. Res.*, in press, 2000.

Lelieveld, J., P. J. Crutzen, and F. J. Dentener, Changing concentration, lifetime and climate forcing of atmospheric methane, *Tellus, Ser. B*, *50*, 128–150, 1998.

Levin, I., and V. Hesshaimer, Refining of atmospheric transport model entries by the globally observed passive tracer distributions of ^{85}krypton and sulfur hexafluoride (SF_6), *J. Geophys. Res.*, *101*, 16,745–16,755, 1996.

Louis, J. F., A parametric model of vertical eddy fluxes in the atmosphere, *Boundary Layer Meteorol.*, *17*, 187–202, 1979.

Maiss, M. L., and I. Levin, Global increase of SF_6 observed in the atmosphere, *Geophys. Res. Lett.*, *21*, 569–572, 1994.

Maiss, M., L. P. Steele, F. R. Francey, P. J. Fraser, R. L. Langenfelds, N. B. A. Trivett, and I. Levin, Sulfur hexafluoride: A powerful new atmospheric tracer, *Atmos. Environ.*, *30*, 1621–1629, 1996.

Matthews, E., I. Fung, and J. Lerner, Methane emission from rice cultivation: Geographic and seasonal distribution of cultivated areas and emissions, *Global Biogeochem. Cycles*, *5*, 3–24, 1991.

Midgley, P. M., The production and release to the atmosphere of 1,1,1-trichloroethane (Methyl Chloroform), *Atmos. Environ.*, *23*, 2663–2665, 1989.

Midgley, P. M., and A. McCulloch, The production and global distribution of emissions to the atmosphere of 1,1,1-trichloroethane (methyl chloroform), *Atmos. Environ.*, *29*, 1601–1608, 1995.

Morris, R. A., T. M. Miller, A. A. Viggiano, J. F. Paulson, S. Salomon, and G. Reid, Effects of electron and ion reactions on atmospheric lifetimes of fully fluorinated compounds, *J. Geophys. Res.*, *100*, 1287–1294, 1995.

Olivier, J. G. J., et al., Description of EDGAR version 2.0: A set of global emission inventories of greenhouse gases and ozone de-

pleting substances for all anthropogenic and most natural sources on a per country basis on 1° x 1° grid, *RIVM Rep. 771060 002/TNO MEP Rep. R96/119*, Natl. Inst. for Public Health and the Environ., Bilthoven, Netherlands, 1996.

Prather, M., M. McElroy, S. Wofsy, G. Russell, and D. Rind, Chemistry of the global troposphere: Fluorocarbons as tracers of air motion, *J. Geophys. Res.*, *92*, 6579–6613, 1987.

Prinn, R. G., et al., Global average concentration and trend for hydroxyl radical deduction from ALE/GAGE trichloroethane (methyl chloroform) data for 1978-1990, *J. Geophys. Res.*, *97*, 2445–2461, 1992.

Prinn, R. G., R. F. Weiss, B. R. Miller, F. N. Alyea, D. M. Cunnold, D. E. Hartley, P. B. Fraser, and P. G. Simmonds, Global weighted-average concentration and trend of OH based on 15 years of ALE/GAGE CH_3CCl_3 data, paper presented at Joint Meeting on Global Atmospheric Chemistry, Int. Assoc. of Meteorol. and Atmos. Phys., Fuji-Yoshida, Japan, 1994.

Prinn, R. G., R. F. Weiss, B. R. Miller, J. Huang, F. N. Alyea, D. M. Cunnold, P. B. Fraser, D. E. Hartley, and P. G. Simmonds, Atmospheric trends and lifetime of CH_3CCl_3 and global average hydroxyl radical concentrations based on 1978–1994 ALE/GAGE measurements, *Science*, *269*, 187–192, 1995.

Ramonet, M., and P. Monfray, CO_2 baseline concept in 3-D atmospheric transport models, *Tellus, Ser. B*, *48*, 502–520, 1996.

Ridgwell, A. J., S. J. Marshall, and K. Gregson, Consumption of atmospheric methane by soils: A process-based model, *Global Biogeochem. Cycles*, *13*, 59–70, 1999.

Russell, G., and J. Lerner, A new finite-differencing scheme for the tracer transport equation, *J. Appl. Meteorol.*, *20*, 1483–1498, 1981.

Saeki, T., T. Nakazawa, M. Tanaka, and K. Higuehi, Methane emissions deduced from a two-dimensional atmospheric transport model and surface measurements, *J. Meteorol. Soc. Jpn.*, *76*, 307–324, 1998.

Sanderson, M. G., Biomass of termites and their emissions of methane and carbon dioxide: A global database, *Global Biogeochem. Cycles*, *10*, 543–557, 1996.

Tans, P. P., A note on isotopic ratios and the global atmospheric methane budget, *Global Biogeochem. Cycles*, *11*, 77–81, 1997.

Tiedke, M., A comprehensive mass flux scheme for cumulus parameterization in large-scale models, *Mon. Weather Rev.*, *117*, 1779–1800, 1989.

Tobler, W., Population database of the Consortium of International Earth Science Information Network (CIESIN) and the Environmental System Research Institute, Inc. (ESRI), through the National Center for Geographic Information and Analysis, *NCGIA Tech. Rep. TR-95-6*, Dep. of Geogr., Univ. of Santa Barbara, Santa Barbara, Calif., 1995.

United Nations, 1992 energy statistics yearbook, *United Nations Publication Sales E/F. 94XVII.9*, Dep. for Econ. and Social Inf. and Policy Anal., Stat. Div., New York, 1994.

Valentine, D. W., E. A. Holland, and D. S. Schimel, Ecosystem and physiological controls over methane production in northern wetlands, *J. Geophys. Res.*, *99*, 1563–1571, 1994.

Walter, B., Development of a process-based model to derive methane emissions from natural wetlands for climate studies, Ph.D. thesis, Fachbereich Geowissenschaften der Univ. Hamburg, Hamburg, Germany, 1998.

Walter, B. P., M. Heimann, R. D. Shannon, and J. R. White, A process-based model to derive methane emissions from natural wetlands, *Geophys. Res. Lett.*, *23*, 3731–3734, 1996.

Westermann, P., Temperature regulation of methanogenesis in wetlands, *Chemophere*, *26*, 321–328, 1993.

Whittlestone, S., S. D. Schery, and Y. Li, Pb-212 as a tracer for local influence on air samples at Mauna Loa observatory, *J. Geophys. Res.*, *101*, 14,777–14,785, 1996.

World Meteorological Organization, GAW data, Greenhouse gases and other atmospheric gases, *WMO WDCGG Data Cat. WDCGG 13*, World Meteorol. Org. World Data Cent. for Greenhouse Gases, Japan Meteorol. Agency, Tokyo, 1997.

Worthy, D. E. J., I. Levin, N. B. A. Trivett, A. J. Kuhlmann, J. F. Hopper, and M. K. Ernst, Seven years of continuous methane observations at a remote boreal site in Ontario, Canada, *J. Geophys. Res.*, *103*, 15,995–16,007, 1998.

Yienger, J. J., and H. Levy, Empirical model of global soil-biogenic NO_x emissions, *J. Geophys. Res.*, *100*, 11,447–11,464, 1995.

F. J. Dentener, S. Houweling, and J. Lelieveld, Institute for Marine and Atmospheric Research Utrecht, Utrecht University, Princetonplein 5, 3584 CC Utrecht, Netherlands. (f.j.dentener@phys.uu.nl; s.houweling@phys.uu.nl; j.lelieveld@phys.uu.nl)

E. J. Dlugokencky, NOAA Climate Monitoring and Diagnostics Laboratory, 325 Broadway, R/E/CG1, Boulder, CO 80303.

B. Walter, Columbia University/NASA Goddard Institute for Space Studies, 2880 Broadway, New York, NY 10025.

(Received August 11, 1999; revised November 22, 1999; accepted November 30, 1999.)